IEEE Access
Multidisciplinary | Rapid Review | Open Access Journal

Received February 19, 2020, accepted March 2, 2020, date of publication March 31, 2020, date of current version April 16, 2020.

Digital Object Identifier 10.1109/ACCESS.2020.2984606

Micro Motion Amplification–A Review

MICHAIL E. KIZIROGLOU[1,2], (Senior Member, IEEE), BURAK TEMELKURAN[2], ERIC M. YEATMAN[1], (Fellow, IEEE), AND GUANG-ZHONG YANG[2]

[1]Department of Electrical and Electronic Engineering, Imperial College London, London SW7 2AZ, U.K.
[2]The Hamlyn Centre for Robotic Surgery, Imperial College London, London SW7 2AZ, U.K.

Corresponding author: Michail E. Kiziroglou (m.kiziroglou@imperial.ac.uk)

This work was supported by the Engineering and Physical Sciences Research Council (EPSRC) under Grant EP/P012779/1.

ABSTRACT Many motion-active materials have recently emerged, with new methods of integration into actuator components and systems-on-chip. Along with established microprocessors, interconnectivity capabilities and emerging powering methods, they offer a unique opportunity for the development of interactive millimeter and micrometer scale systems with combined sensing and actuating capabilities. The amplification of nanoscale material motion to a functional range is a key requirement for motion interaction and practical applications, including medical micro-robotics, micro-vehicles and micro-motion energy harvesting. Motion amplification concepts include various types of leverage, flextensional mechanisms, unimorphs, micro-walking / micro-motor systems, and structural resonance. A review of the research state-of-art and product availability shows that the available mechanisms offer a motion gain in the range of 10. The limiting factor is the aspect ratio of the moving structure that is achievable in the microscale. Flexures offer high gains because they allow the application of input displacement in the close vicinity of an effective pivotal point. They also involve simple and monolithic fabrication methods allowing combination of multiple amplification stages. Currently, commercially available motion amplifiers can provide strokes as high as 2% of their size. The combination of high-force piezoelectric stacks or unimorph beams with compliant structure optimization methods is expected to make available a new class of high-performance motion translators for microsystems.

INDEX TERMS Compliant, energy harvesting, flexure, geometrical gain, leverage, MEMS, micro-robotics, motion amplification, motion translation.

I. INTRODUCTION

The continuing evolution of microelectronics since the 1950s has been the cornerstone of information technology development, enabling seamless information processing, storage and transfer. It has also enabled a rapid development of microfabrication and integration techniques, with a wide range of material integration and lithographic tools that have recently reached the sub- 15 nm range. In turn, the combination of these techniques with active materials and integrated moveable microstructures has opened up new capabilities in sensing, actuating and power-generating microdevices. The thickness limitations of planar Si fabrication processes were addressed to a significant extent by the introduction of Micro Electro Mechanical Systems (MEMS) methods, such as thick metal electroplating, up to 100 μm, deep reactive ion etching, and standardized integrated methods such as LIGA (Lithographie, Galvanoformung, Abformung). The emergence of Motion Processing Units (MPUs), which are already abundant due to their presence in virtually all smartphone devices, is indicative of the successful integration of electromechanical sensors into integrated microchips.

While Si integration is currently available or viable for a surprisingly wide range of sensors, the implementation of integrated actuation systems is not as favorable, because actuation usually requires interaction with the macro scale, indicatively in the range of a few millimeters and above. Examples of such applications include robotics, micromotors, precision positioning, displays, microfluidics and the control of optical systems. The typically used actuation mechanisms, for example piezoelectric, electrostatic or electrothermal, provide a direct displacement in the nanometer to micrometer range. This can be increased by applying large electrical fields, for example by using piezoelectric

The associate editor coordinating the review of this manuscript and approving it for publication was Chenguang Yang.

This work is licensed under a Creative Commons Attribution 4.0 License. For more information, see https://creativecommons.org/licenses/by/4.0/

multilayers or by large aspect ratio piezoelectric or electrostatic microstructures. The displacement can be further increased by employing geometrical and dynamic mechanisms, implemented in the micrometer or millimeter scale.

Such motion amplification mechanisms can provide an interface among nanoscale, microscale and millimeter scale systems. They have enabled various technologies including XYZ precision control and micromanipulator tools for medical micro-robotics. Beyond actuating applications, motion amplification mechanisms can improve ultrasonic or vibration coupling at interfaces for sensing, and provide convenient motion translation methods for energy microsystems. In addition, the translation from large-force/small-displacement to small-force/large-displacement motion can be used in sensor systems to improve sensitivity to input force. Finally, microscale motion amplification mechanisms are expected to provide a key missing element for the implementation and controllable testing of micro-robotic systems in real environments.

The desire for large motion in the microscale, in combination with the availability of advanced and mature micromachining methods, has allowed the implementation of a large range of prototype devices and systems, which is diverse in type of active material and operating principle. The rapid development of recent years has already yielded new commercial products beyond the established piezoelectric unimorph or electro-thermal V-beam actuators, in the millimeter scale. In 2008, Ouyang *et al* presented a review of micro-motion systems, following an application-oriented method with an economic impact analysis, suggesting that the combination of piezoelectric elements with compliant structural designs could lead to cost-effective actuators. Since then, rapid progress in materials, devices and system integration, in combination with emerging additive (3D-printing) and subtractive (laser-based) manufacturing methods, have opened up new opportunities for integrated, nanoscale-actuated interactive microsystems.

This paper aims at reviewing and classifying the various motion amplification mechanisms that have emerged from recent research. In addition, it aims at providing a simplified descriptive and quantitative analysis of the physical concepts behind the various motion amplification implementations. In this way, an understanding of fundamental capabilities and limitations of each is obtained. State-of-the art research and commercially available devices are reviewed and compared, and the prospects of motion amplification for micro-actuator, micro-robotic and energy microsystems are discussed. The review is focused on mechanisms that provide significant (i.e. large) motion amplification. Therefore, a comprehensive review of general motion translation systems for sensors and actuators is beyond the scope of this work.

The paper is structured as follows. In Section II a brief overview of piezoelectric, electrostatic and electrothermal actuation mechanisms is presented including their challenges in achieving large direct displacement. In Section III, the general concept of motion amplification at system-level abstraction is introduced, and in Sections IV, V and VI the various methods of motion amplification are reviewed, organized as direct, indirect and dynamic mechanisms respectively. In Section VII, the concept of compliant mechanisms as a systematic method for designing motion amplifiers is overviewed. Finally, conclusions are presented in Section VIII, highlighting key points towards achieving large motion range in the microscale.

II. ACTUATION MECHANISMS

In order to actuate motion in the microscale, a variety of physical mechanisms can be employed. The main mechanisms that have been successfully used in state-of-art microsystems are piezoelectricity, bulk material electrostatic forces, and thermal expansion. Electromagnetic actuators are not favorable in the microscale and for this reason are rarely used. The direct motion range of piezoelectric, electrostatic and electrothermal actuators is very important to the discussion of motion amplification mechanisms, and is therefore overviewed in the following paragraphs.

The piezoelectric effect is based on the polarized nature of interatomic bonds in certain dielectric materials. The application of an electric field affects their lattice constant, thereby providing expansion or contraction. Bulk piezoelectric materials provide a maximum actuating displacement in the order of 0.6 nm per volt of applied field in the field direction, and $0.26 \cdot a_r$ nm per volt of applied field in the perpendicular direction, where a_r is the perpendicular-to-parallel aspect ratio of the material. These correspond to the d_{33} and d_{31} piezoelectric coefficients of soft PZT, which are some of the highest in commercially available piezoelectrics [1]. Single-crystal piezoelectric materials exhibit higher coefficients (e.g. 1.6 nm/V for single-crystal PMN-PT [2]) at the expense of increased fragility and other practical issues.

In order to achieve high displacement at practically usable voltage levels, the electric field can be applied in the short direction of an active material block, thereby increasing displacement by $a_r \cdot d_{31}/d_{33}$, or by using piezoelectric multilayers, which multiply the strain for a given input voltage. Both methods can result in motion output in the tens of nanometers per volt range. For example, the PZT beam of [3] achieves displacement of several micrometers at 300 V, while the Multi Layer Actuators of Cedrat Technologies provide displacements up to 20 μm [4]. The ultimate limiting factor of practically achievable stroke by an active material layer is its tensile strength or dielectric breakdown limit.

Electrostatic actuation is based on the electrostatic force between surface charges on two structures that can move with respect to each other. Charging is achieved by application of an electric potential difference, or by electrostatic induction on a conductive or semi-conductive material. A parallel-plate geometry is usually employed, and the resulting motion can be either parallel or perpendicular to the plate direction. The displacement range is determined by the structure geometry and limitations on the applied voltage due to dielectric

breakdown and the pull-in effect. According to Paschen's law, the air breakdown limit in the gap range of 1-10 μm is in the 300-2000 V range [5]. The pull-in effect restricts stable operation to gap widths above 1/3 of the original size; beyond this limit the gap will close completely [6]. The resulting contact is undesirable due to possible structural damage or breakdown, and also to avoid sticking due to van der Waals adhesion. Devices typically employ cantilever, zipper [7] or comb [6] implementation geometries, to increase capacitance and thereby force [5].

Electrothermal actuation employs the elastic thermal expansion of materials with increased temperature. The thermal expansion coefficient of bulk materials results in low direct displacement. For example, Si and Al exhibit strains of $2.6{\cdot}10^{-6}$ /°C and $25{\cdot}10^{-6}$ /°C respectively. Polymers exhibit higher coefficients, such as 100-200 $\cdot 10^{-6}$ /°C for polyethylene, but their high elasticity hinders coupling of their motion with other microsystem materials. Electrothermal actuators are typically used in V-beam or unimorph structures [8] to increase displacement, as will be discussed in Sections V.A and V.C of this paper.

A wealth of other actuation mechanisms has been proposed for micro- and nano-scale actuation, including liquid crystal polarization, ionic gels and fluids, surface tension, shape-memory alloys, photo-actuation based on photo-induced charge accumulation at interfaces or on photothermal effects [9], and chemical actuation. A review of such mechanisms, with emphasis on soft actuators, has recently been performed by Hines *et al* [10]. Magnetostriction and electrostriction have also been proposed, with the latter showing significant promise for long aspect ratio devices [11].

While the motion range of these mechanisms is suitable for sensor applications, actuation typically requires a much larger range, often in the mm scale and beyond. For this reason, a variety of mechanical motion amplification systems has been proposed, studied and is currently used in key technologies including biomedical microgrippers, micro-mirror scanning displays, microscopy, and high precision positioning systems. A detailed overview of these methods including conceptual analysis, research and application examples is presented in the following sections.

In order for an actuation mechanism to be usable for mm-scale displacement through a motion amplification system, it must be capable of providing a non-trivial amount of power, operate at reasonable speed, indicatively in the 1 Hz order of magnitude or better, and offer mature and controllable fabrication techniques, compatible with the micro-machining state-of-art. For these reasons, the actuation mechanisms that are commonly used in motion amplification systems are piezoelectric, electrostatic and electrothermal. It should also be noted that in the microscale, most mechanisms use flexing supports rather than sliding or rolling as commonly employed in conventional engineering, due to surface tension limitations and difficulties of lubrication.

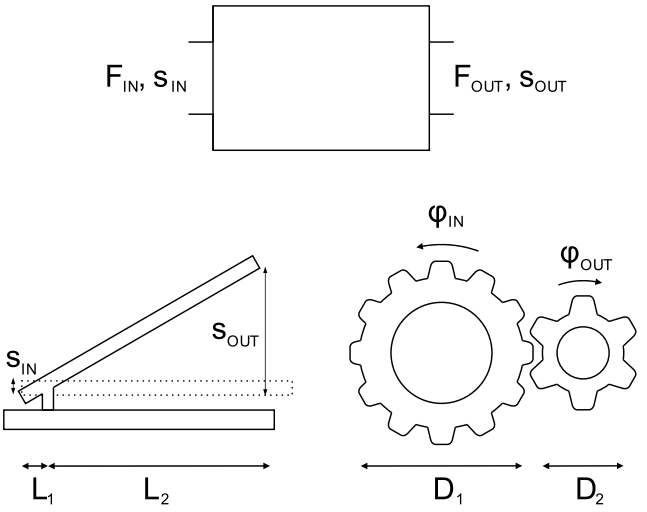

FIGURE 1. Top: Block diagram of a force and displacement transmission system. Motion amplification aims at increasing displacement at the expense of force reduction (geometrical advantage). Force amplification increases the force at the expense of a smaller stroke (mechanical advantage). Bottom: Conventional linear (left) and rotational (right) examples of motion amplification by leverage and gearing respectively.

III. MECHANISMS FOR MOTION AMPLIFICATION

A motion amplification system translates an input motion with a given pair of displacement s_{IN} and force F_{IN} to a new motion with displacement s_{OUT} and force F_{OUT}. This is illustrated in Fig. 1:top. In the general case, the input and output are functions of time, and assuming linearity the system transfer function is a complex matrix, dependent on input frequency. The system can also store and dissipate mechanical energy. Dynamics play an important role in performance and reliability of such systems, but they are very specific to implementations. In order to allow for a simple-to-use analysis and comparison of the very diverse range of amplification techniques, in this paper, the following simplifications are made:

1) The transfer function of motion amplitude, s_{out}/s_{in} is assumed to be a real, constant number, g, independent of the input. This is called motion amplification ratio or geometrical gain.
2) The systems do not dissipate or store mechanical energy. Therefore:

$$\oint F_{IN}\, ds_{IN} = \oint F_{OUT}\, ds_{OUT} \tag{1}$$

3) The effect of adding a mechanical load to the output is not considered. The consideration of the different mechanisms is performed under zero load conditions.
4) The discussion focuses on geometrical gain. The force (mechanical) gain or reduction is not considered.

As an example, the simple lever mechanism, illustrated in Fig. 1:bottom, left, provides a geometrical gain of:

$$g = \frac{s_{OUT}}{s_{IN}} = \frac{L_2}{L_1} \tag{2}$$

Similarly, for a simple gearing mechanism, the geometrical gain, expressed in rotation angles is given by:

$$g = \frac{\varphi_{OUT}}{\varphi_{IN}} = -\frac{D_1}{D_2} \quad (3)$$

When necessary, non-linear or dynamic effects may still be discussed in this review. For example, in the case of amplification by mechanical resonance, the geometrical gain is highly frequency dependent. In addition, in Section VII, the generic system design method of compliant mechanisms is discussed, where the general case of a complex transfer function may be used.

Many practical systems employ complexities such as multiple amplification structures in a single implementation. Here, a mechanical concept-based categorization is attempted, grouping the various mechanisms into the following three types: Direct leverage, Indirect Leverage and Dynamic Motion Amplification. Direct leverage includes simple lever structures. Indirect leverage includes beam buckling and V-shaped beams, interfacial asymmetries, lattice strain mismatch (Unimorph), flextensional mechanisms and the Scott-Russel mechanism. Dynamic amplification includes fast-repeatable motion cycles such as micro-walking and micro-motors, and resonance motion amplification. These motion amplification mechanisms are reviewed in the following sections.

IV. DIRECT LEVERAGE

Different MEMS lever structures have been implemented to amplify the stroke of piezoelectric actuators. In [12], a single-crystal PMN-PT active material is used to achieve amplification from 1 nm to 7 nm at 1 V, for aircraft applications. A MEMS leverage mechanism demonstrating 12 μm displacement from a PZT actuator driven by a 1 kHz, 20 V amplitude signal is used in [13] as a flow modulation valve. Mechanical resonance may have contributed to the large amplification ratio of this device. This mechanism is discussed in Section VI.B of this paper. At a larger scale, in [14] 3D printed Ti alloy levers are employed, demonstrating a geometrical amplification of 6, with a 50 μm motion range, from piezoelectric actuator devices with up to 10 μm stroke at 150 V. The technology is used to implement an XY nano-positioning stage.

MEMS leverage has also been used in electrostatic actuators. In [15], leverage is used to control mirror rotation for scanner arrays. Electrostatic comb actuators are used on the short end of the levers, thereby obtaining a larger stroke on the mirror. A $\pm 6.7^{o}$ rotation is obtained at 75 V. In [16], an out-of-plane displacement of 1.45 μm from a simple parallel plate electrostatic actuation at 47 V is reported, using a leverage with a geometrical gain of 2. An SEM image of this device is shown in Fig. 2. In [17], an electrostatic comb structure is combined with a $\times 2.8$ lever, achieving 60 μm of displacement at 80 V by a 5.5 mm $\times$ 6.0 mm microgripper. A simple $\times 3$ seesaw leverage MEMS structure has also been used for configurable capacitors, demonstrating a 0.15 pF – 0.5 pF capacitance range from a 0 – 15 V actuation voltage [18]. An electrostatic relay with 8 μm contact displacement has been reported in [19] using a 0.7 mm long lever structure.

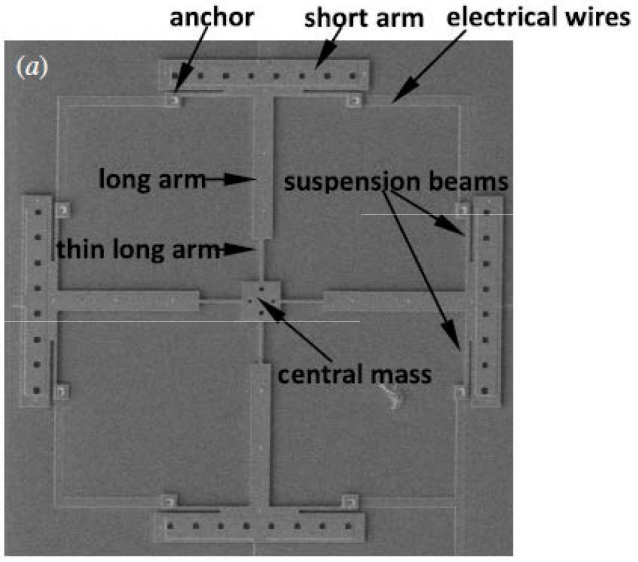

FIGURE 2. A MEMS lever structure with a geometrical gain of 2, by Ren *et al.* from the Chinese Academy of Sciences [16]. ©IOP Publishing. Reproduced with permission.

Electrothermally actuated MEMS levers have also been employed in various systems, usually in combination with other, more complex amplification stages. Such works are reviewed as part of the various other amplification types in the following sections. As a characteristic example, a leverage mechanism with a motion gain of 10 is demonstrated in the electrothermal MEMS of Steiner *et al.* [20].

V. INDIRECT LEVERAGE

A. BUCKLING AND V-SHAPED BEAMS

An indirect method of leverage is using the buckling of a flexible beam. A geometrical description is shown in Fig. 3 top-left. When a lateral force is applied by an active material (red in Fig. 3), asymmetry in the stress distribution can result in perpendicular deformation. A small longitudinal displacement Δx results in a larger perpendicular displacement Δy, thereby providing motion amplification.

An implementation variant of the bending beam mechanism is the V-beam actuator, where a V-shaped beam is used instead of an arc deformation. In many implementations, a flexure hinge is employed, as shown in Fig. 3: top-right. This structure is called a flextensional [21] or bridge-type [22] motion amplifier and can comprise more than one flexure. For a single hinge at the beam center, because the deformation concentrates at the hinge the amplification gain can be calculated by assuming a triangular geometry.

An analysis of this simplified geometry is presented in Fig. 3: bottom. At a given bending angle θ_1 and at constant V-shape leg length L, an infinitesimal longitudinal displacement dx results in a perpendicular

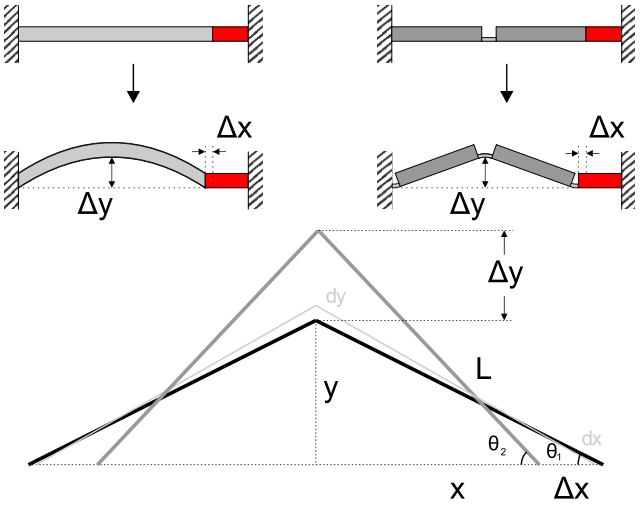

FIGURE 3. Top-left: Beam deflection results in motion amplification between the longitudinal and vertical directions. Top-right: The bridge-type flextensional implementation. Bottom: Geometrical analysis assuming a triangular geometry, for bending from a starting angle, θ_1 to an angle θ_2. The bold black and grey lines represent the starting and final positions respectively. The thin grey line shows an infinitesimal angle change with displacements dx and dy.

displacement dy such that:

$$g = dy/dx = -x/y = -cot\theta_1 \tag{4}$$

where g represents the geometrical advantage. Eq. (4) can be used as the displacement gain for small Δx values. For larger displacements resulting in angle change from θ_1 to θ_2, the geometrical gain can be found by integration, giving:

$$g(\theta_1, \theta_2) = -cot((\theta_1 + \theta_2)/2). \tag{5}$$

This simplified analysis can be used for the calculation of motion amplification from a single–flexure geometry. In addition, it can provide an approximate first estimate for deflected beam structures, for small input displacements. In practice, complex bridge structures and other geometries are used, often in applications where precision is a key objective. Therefore, more accurate analyses and simulation techniques are required. Flextensional motion amplification devices are discussed in more detail in Section V.D of this paper.

As an example, in a V-Shaped, 3 mm long beam motion amplifier, a gain of around 19 is demonstrated for an optical accelerometer application [23]. This large gain is achieved by operating at a very low angle, around 2 degrees, and by the negligible mechanical load requirement of optical sensing applications. V-Shaped beams are also typically used for motion amplification of electrothermal actuators, but with the active element along the L-long hypotenuse of the triangle in Fig. 3: bottom, giving a displacement of dL at constant x. In this case, the geometrical gain is:

$$g = dy/dL = sin^{-1}\theta \tag{6}$$

Gain values over 5 are given for angles lower than 20°. In this range, the gain is practically identical to that

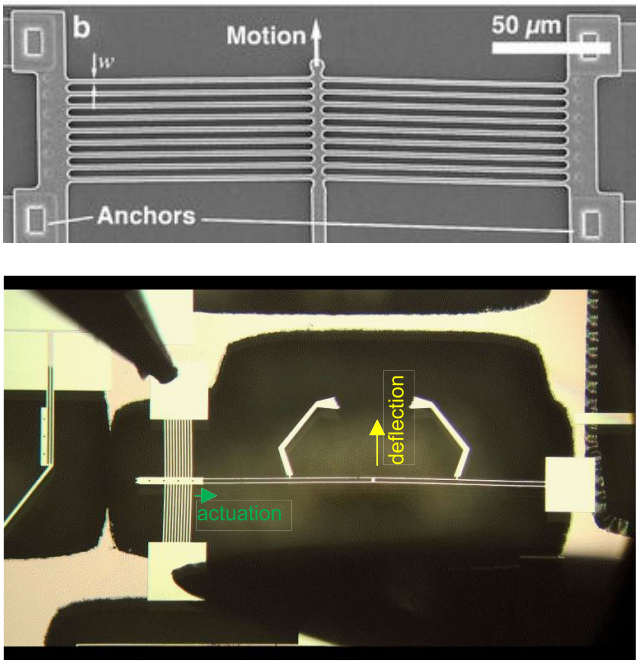

FIGURE 4. Top: Example of electrothermal chevron MEMS actuator by Brown and Bright, ©Springer. Reproduced with permission [25]. Bottom: Example of electrothermal actuator in combination with a deflecting beam from the nanofabrication laboratory of the University of Utah [26], Reproduced with permission.

of Eq. (4). In electrothermal actuators, multiple thermally expanding V-beams are used in parallel, in a chevron-like geometry, for higher actuation force [24]. An electrothermal chevron structure example is shown in Fig. 4: top, by Brown and Bright [25].

On the bottom of Fig. 4, a combination of such an actuator with a secondary beam-deflection amplification stage, by the nanofabrication laboratory of the University of Utah, is shown [26]. In this group, various other interesting actuating structures have been developed for educational purposes [26].

In combination with a lever and employing a misalignment method to apply the chevron actuator displacement very near the lever rotation center, in [27] a total geometrical gain of 85 is reported. In the work of Bergna *et al.* for nano-positioning systems, a MEMS chevron structure is implemented for a thermal actuator, demonstrating displacement of 5 μm [28]. This displacement is further amplified by flexure structures to strokes up to 80 μm [29].

A similar nano-positioning system with an 83 × 83 μm displacement capability was also reported in [30]. As mentioned, flexure based structures are discussed in Section V.D of this paper. Another thermally-actuated V-beam implementation for MEMS optical switching obtaining a maximum stroke of 200 μm is reported in [31]. Similar structures in combination with buckling beams have also been proposed for bi-stable MEMS switches [32]. Finally, in [20] a V-beam thermal actuator device has been developed, achieving displacement of around 50 μm from environmental temperature change

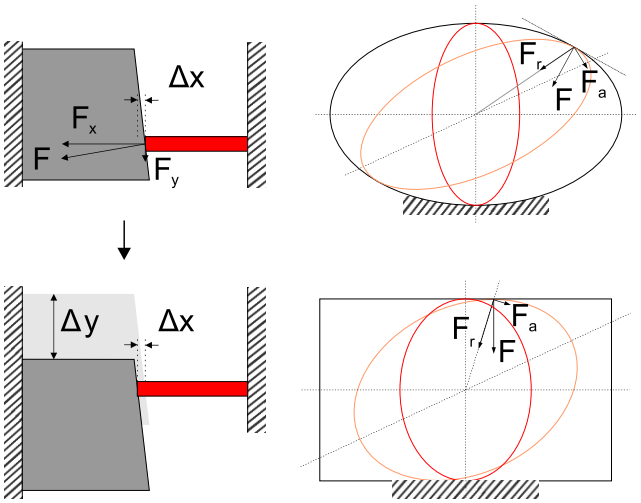

FIGURE 5. Motion transmission by tangential stress. Left: Concept description. Right: Conceptual illustration of an implementation using stress between two elliptical structures (right-top) and an elliptical in a rectangular structure (right-bottom).

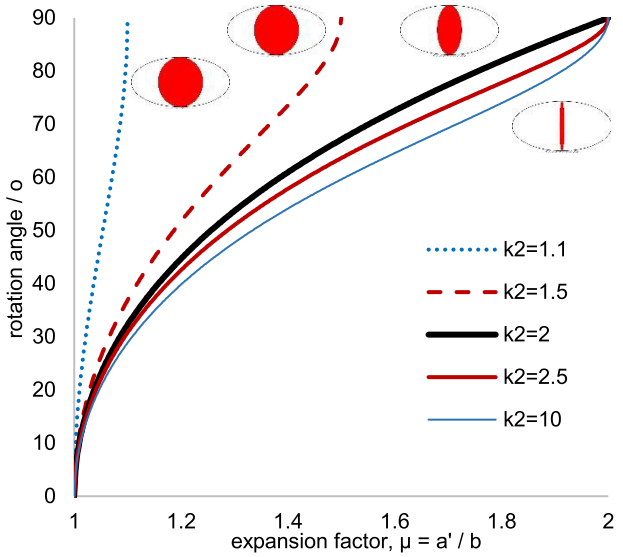

FIGURE 6. Calculated rotation due to expansion of an elliptical cylinder confined in a rigid elliptical box (Fig. 5, right, top), using Eq. (5). Sharper rotation occurs for smaller k_2. The required expansion factor for right angle rotation is equal to k_2.

between ±35 °C. The thermal expansion of the 0.4 mm long Ni beams that are used is 5 nm/K and is amplified by the V-beam and a MEMS lever, each providing a motion gain of around 10. This novel approach is proposed for passive temperature sensing. A magnetostriction-based chevron V-beam actuator has also been proposed by the same group in [33], demonstrating displacement output of 10 μm, by the application of a 14 mT magnetic field. The overall size of this device is 4 × 2 × 0.4 mm.

B. INTERFACIAL ASYMMETRIES

Another possible leverage-based motion amplification mechanism is obtained by employing the interfacial forces between two surfaces pressing against each other due to expansion. The forces are perpendicular to the interface tangential surface, and depending on the resting geometry can induce a linear or rotational motion. A linear motion example is illustrated in Fig. 5 (left). The angle between the interface tangent and the resting orientation determines the relation between the expansion displacement Δx and the linear displacement Δy. The geometrical advantage will be $g = cot\theta$, similarly with other cases.

One rotational motion example is the case of an elliptical cylinder confined and abiding to a larger elliptical cylinder or parallelepiped, as illustrated in Fig. 5 right top and right bottom respectively. Expansion of the internal ellipsoid results in interfacial force at an angle with the radial plane, and hence in a net torque, causing the ellipsoid to rotate. The rotation angle obtained by a given expansion displacement can be calculated analytically in two dimensions from the equation system of the two cross-section curves and the condition of a single solution in the y-positive half plane. In the case of an elliptical enclosure of a and b large and small semi-axes respectively, if a' and b' are the large and small semi-axes of the inner ellipse, the abutment condition at a rotation angle θ from the vertical orientation gives:

$$cos^2\theta = \frac{(a^2 - a^2) \cdot (b'^2 - b^2)}{(a^2 - b^2) \cdot (a^2 - b^2)} \tag{7}$$

A parametric analysis of this system is possible by defining $k_1 = a/b$, $k_2 = a'/b'$ and assuming an initial internal ellipse large axis $a'_0 = b$, such that the factor $\mu = a/a'_0 = a/b$ corresponds to the expansion ratio. At $\mu = 1$ the ellipse is at the vertical position and Eq. (4) can be written as:

$$cos^2\theta = \frac{(k_1^2 - \mu^2) \cdot (k_2^2 - \mu^2)}{\mu^2 \cdot (k_1^2 - 1) \cdot (k_2^2 - 1)} \tag{8}$$

For these parameters, the following restrictions apply: $k_1, k_2 \geq 1$ and $1 \leq \mu \leq k_1$. As an example, results of θ versus μ, for a case of $k_1 = 2$ and varying k_2 are shown in Fig. 6.

If $k_2 \geq k_1$, i.e. if the internal ellipse is more eccentric, the rotation maximum $\theta = 90^o$ is achieved when $\mu = k_1$. This corresponds to the three solid lines in Fig. 6. When $k_2 < k_1$, maximum rotation is achieved when $\mu = k_2$. In practice, this means that the required expansion for 90^o rotation is determined by the internal ellipse fabrication method accuracy. For example, a fabricated ellipse with semi axes ratio of $k_2 = 0.001$ is expected to rotate by 90^o when it expands by a factor of 0.001. In other words, if an ellipse confined in its long direction expands such that its short semi axis becomes equal to the initial long semi axis length, it exhibits right angle rotation. The case of a rectangular enclosure corresponds to that of an ellipse with very large k_1.

The method described in this section has not been employed in practice for motion amplification, and while sliding or rolling engineering in the microscale is challenging,

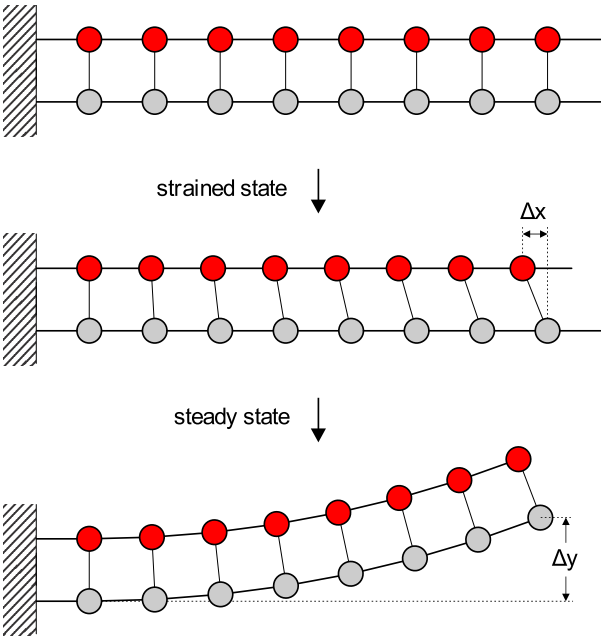

FIGURE 7. Motion amplification due to lattice strain mismatch. The vertical lines do not necessarily represent the atomic layer but rather, they represent general adhesion.

it is foreseen as a promising method for the near future. Afterall, a variant of this method has been employed in micro-motor devices, where a frame-confined piezoelectric disc is excited in various modes, resulting in continuous rotational motion [34]. This type of micro-motor is called a hula-hoop or wobble motor.

C. LATTICE STRAIN MISMATCH (UNIMORPH)

The use of a unimorph (or bimorph) is one of the most common methods for motion amplification in millimeter scale actuators. A structure that includes one active and one passive layer is called a unimorph, while a structure with two active layers is called a bimorph. Their operating principle is based on the different lattice constant contraction factor between materials, in response to an actuating mechanism such as the application of an electrostatic field (piezoelectrics), a magnetic field or a temperature change. A stack of an active and a passive material is fabricated in a beam structure. The lattice constant strain mismatch induced by the actuation mechanism results in stress at the interface which is relaxed in a bending orientation. This mechanism is graphically described in the atomic level in Fig. 7. The horizontal bonds are shown to demonstrate the effect of contraction difference, while the vertical bonds provide a picture of local adhesion between the two layers. Therefore, the vertical lines do not necessarily represent atomic layer bonds, and in any case are not meant to suggest an epitaxial interface.

In practice, the displacement of a unimorph depends on material properties, fabrication method and interface quality as well as on the structure shape and dimensions. For unimorph design and performance prediction, beam theory and material simulation are typically employed.

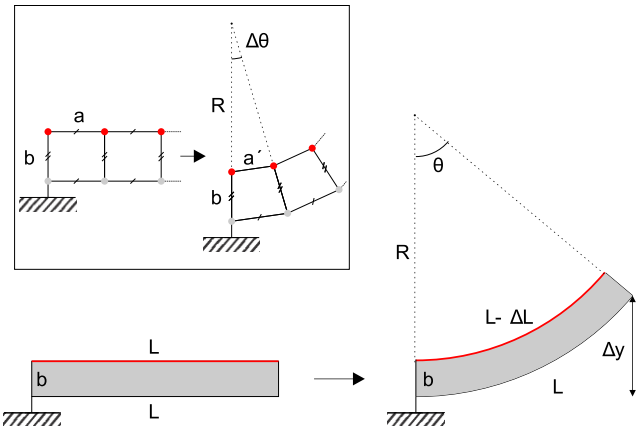

FIGURE 8. Geometrical calculation of motion amplification achieved by a unimorph. In the inset, the corresponding calculation assuming an active and an uncompressed atomic monolayer at a constant distance b is illustrated.

The deflection of different beam geometries and mounting cases in response to a given applied force, or to a specific actuation mechanism, can be calculated analytically (e.g. the analysis of Timoshenko in [35]). For an estimation of motion amplification capability, a simple geometrical analysis can be employed. In such an analysis, the deflection angle θ and vertical displacement Δy are sought. An unmounted unimorph of length L and thickness b is considered, bendable in the y direction. In this consideration, the strain along the direction of b can be neglected and the bottom beam length is considered constant. This is illustrated in Fig. 8. In practice, the bottom beam length expands and therefore b can be considered as the depth of the zero-strain plane (neutral axis) of the beam. This is not illustrated in Fig. 8, for geometrical simplicity.

The structure has the same cross-section along the z-direction (i.e. perpendicular to the paper in Fig. 8) and therefore the analysis can be performed in two dimensions. Assuming a constant bottom length, negligible thickness compression and negligible edge effects, an active layer shrinking by ΔL results in a circular bending as shown on the right of Fig. 8. The top side arc will have a radius R and a length of L-ΔL, while the bottom side arc will have a radius of R+b and a length of L. The total bending angle and vertical displacement with then be:

$$\theta = \frac{\Delta L}{b} \tag{9}$$

$$\Delta y = \frac{L}{\theta} \cdot (1 - cos\theta) \tag{10}$$

The same result is derived by considering an active and a passive, uncompressible atomic monolayer, mounted together by uncompressible but rotatable bonds. This orientation is shown in the inset of Fig. 8, and it also corresponds to accordingly bonded structural blocks. A top layer lattice constant shrinkage by $\alpha' - \alpha = \Delta x$ results in trapezoidal cells with top and bottom sides of a' and a respectively and equal lateral sides of b. Every cell contributes to a rotation of

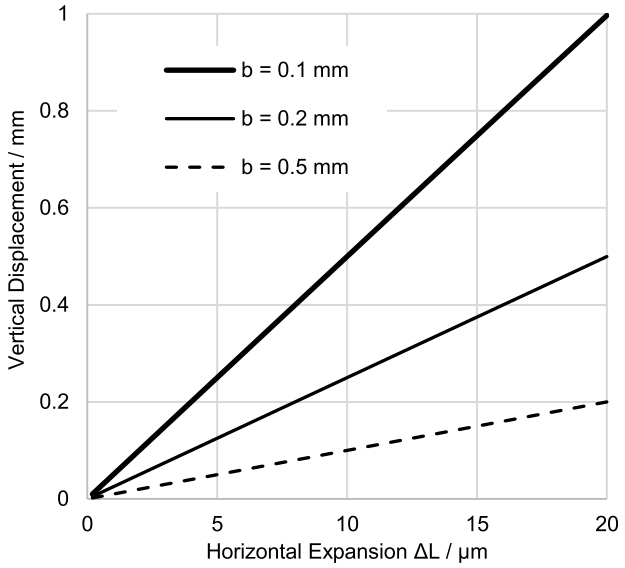

FIGURE 9. Vertical displacement of a unimorph as a function of shrinkage for different unimorph thicknesses b, calculated from Eq. (10).

the structure by $\Delta\theta$ such that:

$$\sin\frac{\Delta\theta}{2} = \frac{\Delta x}{2b} \tag{11}$$

In the case of small $\Delta\theta$ and a large number of cells giving a total shrinkage of ΔL, this corresponds to Eq. (9). It is noted that the length b remains the same because in both the beam and the atomic scale, b is the distance between the active layer and the zero-strain layer.

An analytical expression of the geometrical gain can be calculated for small deflection angles θ from Eqs. (4) and (5), using a 2nd order Taylor series approximation for cosθ:

$$g = \frac{\Delta y}{\Delta L} = \frac{L}{2b} \tag{12}$$

Indicatively, the vertical displacement versus horizontal shrinkage ΔL as calculated from Eq. (10) is plotted for three different values of b in Fig. 9. The selection of values and scale is based on realistic beam thicknesses (or zero-strain plane depths) and active layer expansion that would provide useful geometrical gain. A geometrical advantage of over 10 can be obtained by unimorphs with thickness below 0.5 mm.

A variety of lattice strain mismatch-based devices has been studied in the literature and used mainly in actuating, sensing and energy harvesting applications. They typically have one or two (bimorph) active material layers deposited on a passive substrate. Most often, the active materials are ether thermal expansion based or piezoelectric. Thermally actuated unimorphs have been extensively used as electrical switches and fuses. New fabrication techniques have recently enabled new structures and an expansion of applications. For example, electrothermal actuation of polyethylene by printed conductive heating elements has been demonstrated by Felix Heibeck *et al.* from the MIT Media Lab, showing impressive bending performance and various application possibilities [8]. Results show bending of a 25 mm long device at an angle of 140°.

Piezoelectric cantilever beams have been used as accelerometers in discrete component form, or as MEMS systems. They have also been integrated with electronics into so-called motion processing units. As a long displacement actuation example, in [36] a 0.5 μm PZT / 1 μm SiO_2 cantilever is reported, achieving 150° of rotation and 950 μm maximum displacement from a 15 V bias. Taking into account the 1.5 mm beam length and assuming a d_{31} of 0.26 nm/V, the PZT expansion would be 12 μm. Therefore the 950 μm output displacement corresponds to a geometrical gain of 80. In [37], a 34 mm long, 4.5 μm PZT / 16 μm aluminium beam is shown to achieve a quasi-static deflection of 750 μm at 10 V. Assuming again a d_{31} of 0.26 nm/V, the PZT expansion would be 20 μm, corresponding to a geometrical gain of 37.5. In practice, typical commercially available discrete piezoelectric beam devices demonstrate much lower strokes at this voltage, in the range of tens of μm, due to the thicker substrate used in order to ensure a reliable rigidity [38].

Beam deflection systems using other actuation mechanisms have also been proposed. A new, electrostatic approach using the flexure of a Λ-shape vertical patterned layer with underlying airgap has been proposed in [39], showing tip displacement of around 0.3 μm at 45 V. Recently, an electrostrictive material with strain performance as high as 8% at 200 V has been employed in a unimorph system, demonstrating deflection of a 35 mm long fiber by 80 μm [11]. Based on the 1.3 μm active material contraction, this corresponds to a unimorph-generated geometrical gain of 61.5.

The majority of applications for unimorphs and bimorphs regards sensing, actuating and robotic functionality. The performance priorities for the former are linearity and sensitivity, while reliability and large displacement are more important for the last two. In addition, unimorphs and bimorphs have been extensively studied as motion transducers for micro-energy harvesting applications [40]–[42]. In energy applications, low-frequency, broadband and high amplitude operation is desirable, making non-linear materials and architectures preferable [43]. Furthermore, non-toxic and flexible active materials are currently key research priorities for all the aforementioned applications.

Despite their high geometrical gain, the small achievable final stroke of lattice strain mismatch devices limits their usage in larger scale actuation applications. However, the high force that is achieved by these devices makes their combination with other motion amplification structures such as flextensional and compliant mechanisms very attractive. These mechanisms are discussed in Sections V.D and VII of this paper.

D. FLEXTENSIONAL MECHANISMS

A popular method for amplification of piezoelectric motion is to use an asymmetric frame such as a rectangle, a rhombus, or an ellipse. The piezoelectric displacement is applied to the

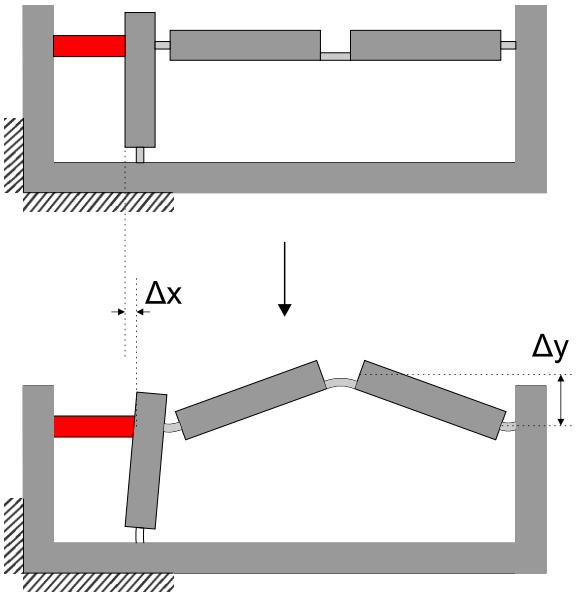

FIGURE 10. Flextensional motion amplification concept.

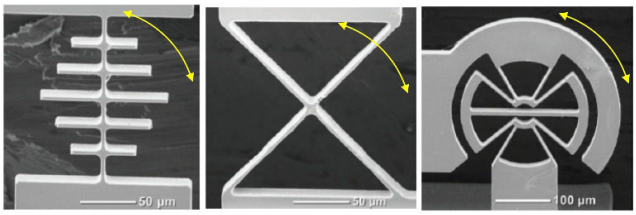

FIGURE 11. Beam, cartwheel and butterfly MEMS flexures developed by Kim *et al.* [29] ©IOP Publishing. Reproduced with permission.

long axis of the frame, which results in a larger displacement on the short axis, in the same manner as with the deflection of a beam discussed in Section V.A. This concept is illustrated in Fig. 10.

The flexibility of the frame can originate from the elasticity of the material used, from hinges placed at corners, or from fabricated flexures along the frame. The flexures can be designed according to motion type, stiffness, durability and linearity specifications as well as to observe out-of-plane deformation limits. Performance prediction and optimization can be accomplished using general purpose numerical simulation software. A characteristic example of optimized linear and rotational MEMS flexures is the Si flexures of Kim *et al.* shown in Fig. 11 [29].

Implemented flextensional geometries include elliptic, rhomboidal, moonie, rainbow, cymbal and orthogonal frames, frames with bridge-type flexures as discussed in Section V.A, as well as combinations of shapes, and 3D motion designs. A classification of such structures from Ling *et al* is illustrated in Fig. 12 [21].

3D implementations in particular can achieve stroke amplifications as high as 30 [44] (or over 40, by fabrication of theoretically studied and optimized bridge structures, [45]), because they effectively involve two stages of amplification.

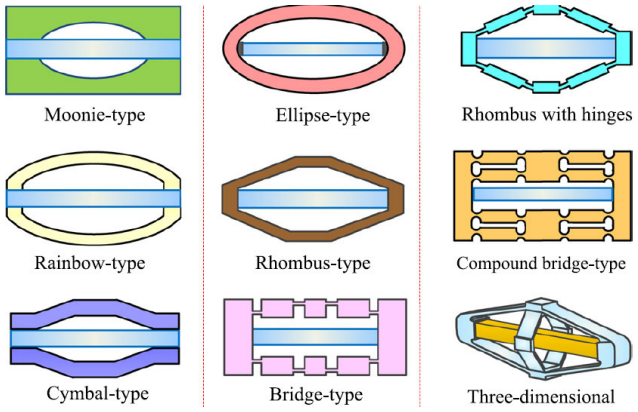

FIGURE 12. Classification of flextensional motion amplification structures from Ling *et al.* [21]. ©IOP Publishing. Reproduced with permission.

Negative stiffness mechanisms have also been proposed to neutralize the dynamic energy stored in the flextensional mechanism and thereby increase the energy transfer efficiency [46]. Structures incorporating bridge-type amplification with additional amplification stages such as leverage have also been reported [22], [47].

For a given geometry, the motion and force translation relationships can be calculated. For example, for a rhomboidal frame of dimensions x and y, rigid beam sides and hinged corners, the calculation of geometrical advantage gives the solution of Eqs (2) and (3). As discussed, this triangular geometry analysis can be useful as an approximate estimate of motion amplification for more shapes and more complex structures. However, in a variety of flextensional device applications, precision of motion is highly desirable, and for those, calculations of higher accuracy are required. Such applications include nano-positioning XY stages [48]–[50], controllable tilting for micro-manipulation equipment [51] and microgrippers [52], including those equipped with force-control [53].

In order to optimize the design of flextensional devices, various analytical and numerical models have been developed. These studies employ the elastic beam theory and kinematics to derive mathematical models of performance [54]–[56]. Enhanced analytical models for bridge and rhombus type structures have been proposed in [21]. An overview of flextensional geometries is presented and a mathematical model allowing simplification to a rhombic structure analysis is introduced. Studies on the maximization of bridge-type amplification [57], [58], kinematic analysis for nano-positioning stages [59], flexure stress and fatigue [60], as well as on the effect of the mechanical load on device performance [61] have also been reported. A more holistic approach for design optimization of compliant mechanisms has been introduced in the work of Lobontiu [62] and Lobontiu and Garcia [63]. An overview of this approach is presented in section VII of this paper.

A microgripper implementation has recently been reported by York *et al.*, achieving a 106 μm free displacement

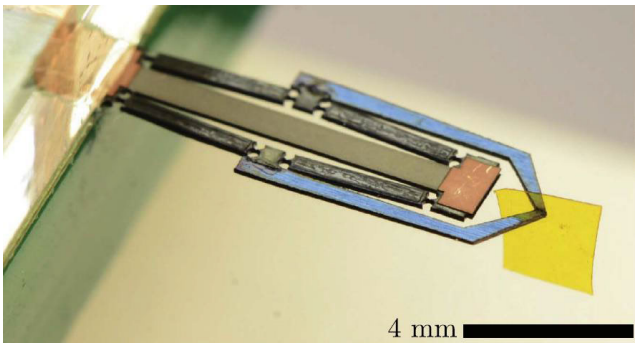

FIGURE 13. The flextensional microgripper from York *et al.* [3]. ©IOP Publishing. Reproduced with permission.

and 73 mN of blocked force, from an 8 mm long piezoelectric beam [3] and 300 V. A photograph of this microgripper illustrating clearly the bridge-and-lever structure combination is shown in Fig. 13. The work in [3] includes an overview of motion amplification mechanisms with discussion and classification focusing on size and energy density performance.

A range of products based on this concept are available on the market, typically using multilayer piezoelectric actuators. Their final stroke depends on the overall device size. The APA series of CEDRAT can provide displacements up to 2 mm between -20 V and 150 V from device sizes up to 139 × 26 × 20 mm (APA2000L) [64]. As a smaller scale example, the APA50 XS bridge uses a 10 × 5 × 2 mm PZT multilayer with 10 μm stroke to achieve 70 μm of no-load displacement output. This corresponds to a geometrical gain of 7 for the bridge structure. Similar performance is provided by a series of other manufacturers. For example, the AP830 actuator of Piezodrive provides a displacement of 830 μm from a -15 V to 150 V voltage range and a 52 × 16 × 14 mm device size [65]. The APF710 actuator of Thorlabs provides a displacement of 1.5 mm between -30 V and 150 V, from a 100 × 18 × 10 mm device, by combination with additional leverage using a flexure structure [66]. The TITAN series of QorTek provides various designs with displacement up to 240 μm and a reported geometrical gain of 12 [67]. A photograph of a device from this series illustrating the monolithically fabricated flexures is shown in Fig. 14 top.

The Dynamic Structures and Materials (DSM) FPA series provides displacement up to 2 mm between -20 V and 150 V, at a size of 96 × 28 × 18 mm [68]. The 134 × 30 × 14 mm NAC2645 from Noliac gives 950 μm displacement at 200 V, utilizing a four-beam structure [69]. Finally, the PI P602 series gives 1 mm of displacement between -20 V and 120 V, at a size of 126 × 34 × 14 mm [70]. All these products employ a flexure design to improve the geometrical gain. Further gain is possible by combination with additional leverage such as in the DSM LFPA series, reaching a displacement as large as 10 mm [71]. A photograph of a DSM LFPA lever-amplified flextensional bridge is shown in Fig. 14: bottom.

A summary of these examples is presented in Table 1. Overall, the amplification gain of commercially available flextensional bridge structures is in the range of 10, substantially smaller than that achieved or predicted in the research state-of-art (e.g. 40 in [45]).

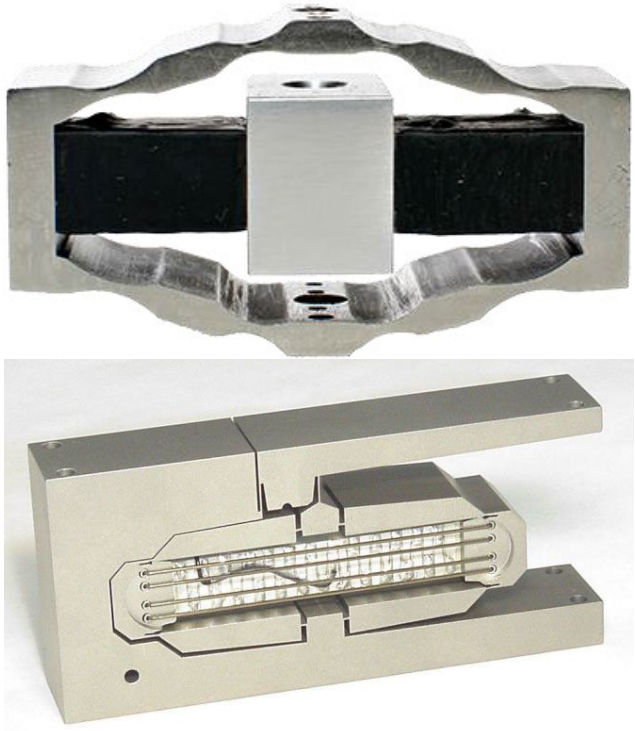

FIGURE 14. Top: Photograph of a QuorTek Titan flextensional bridge [67], courtesy of QorTek, Inc. Bottom: Photo of a DSM LFPA lever amplified flextensional bridge [71], courtesy of Dynamic Structures and Materials LLC. Reprinted by permission.

TABLE 1. Performance of commercially available flextensional bridge motion amplifiers.

Manufacturer / Model	Size / mm	Voltage / V	Stroke / µm
CEDRAT APA 2000L [64]	139 × 26 × 20	-20 to 150	2000
CEDRAT APA50 SX [64]	10 × 5 × 2	-20 to 150	10
PIEZODRIVE AP830 [65]	52 × 16 × 14	-15 to 150	830
THORLABS APF710 [66]	100 × 18 × 10	-30 to 150	1500
QORTEK TITAN [67]	various	-	240
DSM FPA [68]	96 × 28 × 18	-20 to 150	2000
NOLIAC NAC2645 [69]	134 × 30 × 14	0 to 200	950
DSM LFPA [71]	106 × 47 × 20	-30 to 150	10000

E. SCOTT–RUSSELL MECHANISMS

An interesting mechanism to consider in designing leverage devices with flextensional joints is the Scott – Russel, also known as half beam mechanism, which is described

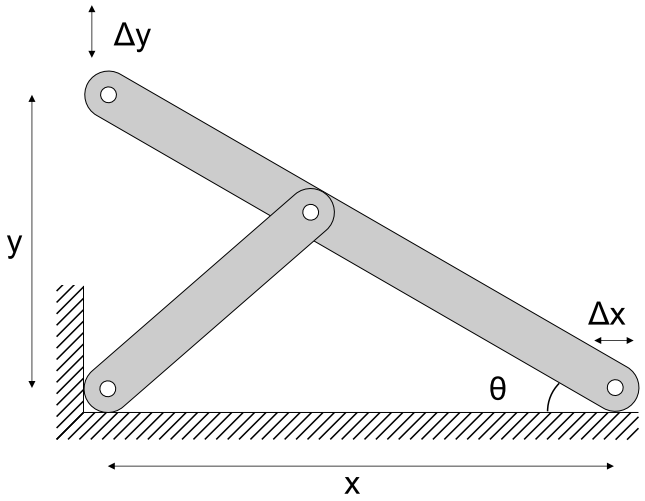

FIGURE 15. The Scott–Russell linear motion translation concept.

geometrically in Fig. 15 [72]. One end of a beam is confined to a linear trajectory (e.g. with a slider joint), while the middle of the beam is linked to a fixed point on the sliding axis with a revolute joint via another beam. If the link beam length L is half the primary beam length, the other beam end follows a linear trajectory perpendicular to the actuating linear motion. This geometry is used for linear motion translation to the perpendicular direction.

As a motion amplification mechanism, the Scott – Russel orientation is a special implementation of the triangular geometry analysis of Section V.A. The geometrical gain is -cotθ, as also shown in [73]. In the work of Ha *et al*, a gain of 2 is experimentally demonstrated [73]. Modifications for different relative dimensions and additional pivotal points have been shown to improve the geometrical advantage while maintaining near-linear output [74]. In [75], a total gain of 6 is achieved by combining a Scott-Russell with a half – bridge structure. The mechanism is used to implement a decoupled XY stage. Studies of this and other linear motion translators/ amplifiers for micro-gripper applications have also been reported [76]. Another combination with a parallel leverage structure with a 3.6 gain has been demonstrated, enabling a microgripper system [72]. Last but not least, Sun *et al* reported a Scott-Russell / leverage mechanism with a combined gain of 15.5 [77]. A photograph of the microgripper device is shown in Fig. 16. In such implementations, flexures take the role of the pin joints of Fig. 15. They offer a pivotal-point mechanism, and their behavior is equivalent to pin joints, at least for small angles.

A more systematic design method for optimized combined structures that can meet predefined motion translation specifications is that of compliant mechanisms, as discussed in Section VII of this paper.

VI. DYNAMIC MOTION AMPLIFICATION

A. MICRO–WALKING AND MICROSCALE MOTORS

Repeated micro-motions obtained by transducers can be converted to long-range linear motion and continuous rotation.

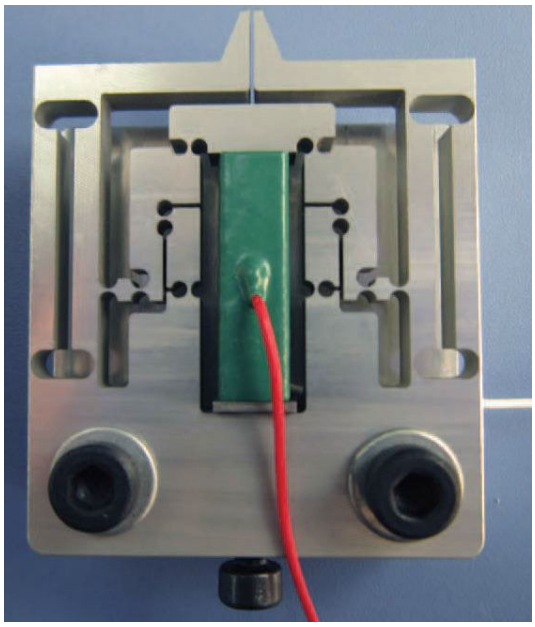

FIGURE 16. The Scott – Russell / leverage mechanism of Sun *et al.* [77]. ©AIP, Reproduced with permission.

Piezoelectric actuators have been proven to be the most suitable for this approach, as their performance supersedes that of electromagnetic transducers in the microscale. In addition, they can operate at high frequencies. Electrostatic implementations using parallel-plate geometries and stepper motor operation as well as potential wave methods have also shown significant promise for micro-motor applications [78]. Furthermore, electrothermal micro-walking devices have been considered, taking advantage of the fast temperature transients in the microscale [79]. Finally, surface tension based hydraulic micromotors have been demonstrated recently, showing significant potential for low-load microactuation [80]. Although micromotors arguably comprise a different field than motion amplification, a brief overview is presented in this paper, because they sometimes find similar applications, such as nano-positioning and xy stage systems.

Piezoelectric motors are based on repeated contraction of an active layer which shifts a movable part in a step-by-step manner. Various mechanisms have been proposed for this purpose, which can generally be categorized into step-sequence devices and ultrasonic motors. Step – sequence devices can use one or more piezoelectric legs to actuate a long range linear motion or rotational motion of a shaft. A variety of walking styles have been adopted, with most exhibiting bidirectional motion capability. As an example, an inchworm-like mechanism is described in Fig. 17. It includes two controllable clamping legs and a contracting body. Linear motion is obtained by successive release of one leg, body extension, re-clamping, release of the other leg, body shrinkage and re-clamping. Similar systems can also be used for rotating motion.

It is also possible to produce bidirectional, repeatable net displacement by pushing a shaft with the tip of a vibrating

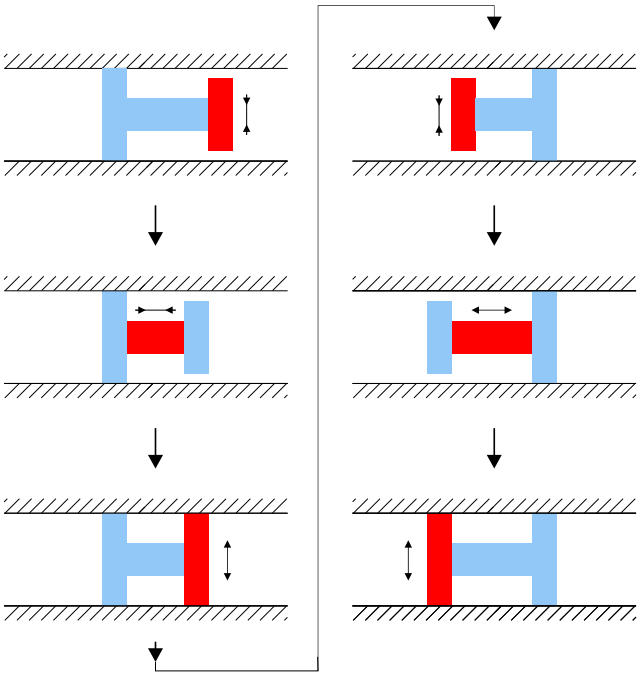

FIGURE 17. The inchworm–like micro-walking motion concept, after Peng *et al.* [81].

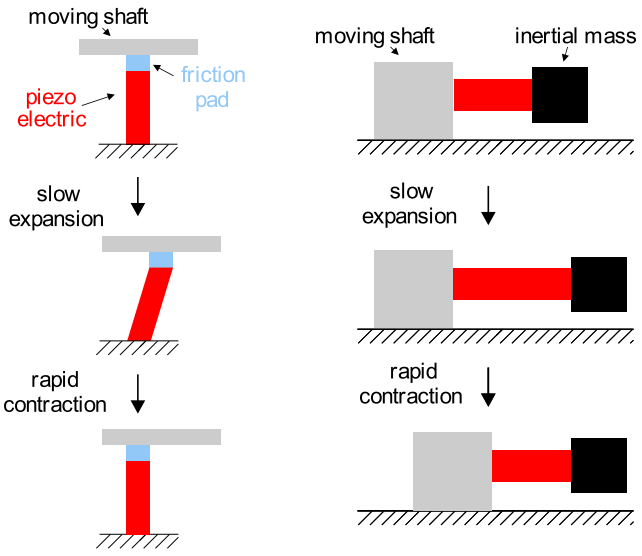

FIGURE 18. Left: Net displacement by asymmetric vibration of a pushing beam. Right: Net displacement by slow and fast motion of an internal inertial mass. After Peng *et al.* [81].

beam with slower motion in one direction. The functionality of this method is illustrated in Fig. 18, left. The forward and backward sweeping speeds of the beam can be selected such that a fast beam motion overcomes the static friction resulting in sliding (no shaft motion), while a slow beam motion drags the shaft. Other implementations exploit the inertia of an internal mass, when pushed rapidly in one direction and slowly in the other (Fig. 18, right). This results in different forward and backward forces appearing on the shaft. The static friction force between the shaft and the

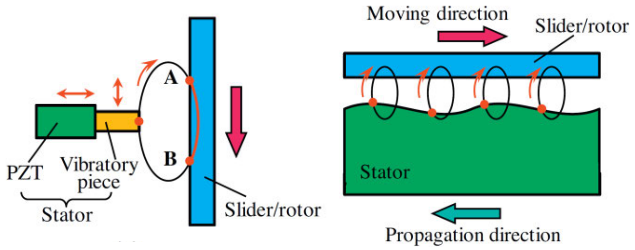

FIGURE 19. Operating principle of standing wave (left) and travelling wave (right) ultrasonic motors. Both images are by Peng *et al.* [81]. ©Elsevier. Reproduced with permission.

stationary surface can block only the weaker, slow proof-mass motion force, resulting again in controllable, bidirectional net motion.

The operation principle of ultrasonic motors is similar in nature to micro-walking but leads to a more systematic exploitation of the actuator motion. The fundamental difference is that motion repetition is obtained in a continuous, analogue manner, as opposed to the discrete steps of micro-walking. The motion-inducing tip(s) of the actuating element(s) follows an elliptical trajectory, typically taking advantage of vibration resonance modes, which can result in unidirectional or bidirectional motion capability. A large variety of ultrasonic motor operating principles have been proposed, with piezoelectric actuation mechanisms in different geometries and sizes, for both linear and rotational motion. They are classified into standing and traveling wave motors, as described in Fig. 19.

In standing wave motors, one or more tips are driven by two perpendicular, harmonic waves resulting in an elliptical trajectory. It is also possible to achieve elliptical motion by the superposition of two natural vibration modes of a stator. Thereby, tip-rotor contact occurs only during one travelling direction, resulting in rotor shift, as shown in Fig. 19, left. The motion direction can be determined by the phase difference between the two signals. An example of special interest is the dual fin device of Friend *et al.* [82]. Two different, passive fins with distinct resonance frequencies are employed, as illustrated in Fig. 20. Bi-directional motion is achieved by exciting the structure with one of the two frequencies. A key advantage of this method is that the stator and the interface fins are passive, providing significant flexibility to device design as well as fabrication simplicity.

In travelling wave motors, a travelling vibrational wave is induced in a stator by applying two actuating signals of perpendicular phase difference [34]. As a result, each surface point follows an elliptical path driving a contacting surface along the opposite-to-the-wave direction, as shown in Fig. 19, right. The main advantages of travelling-wave ultrasonic motors are direct control of motion direction, the use of surface instead of tip contacts, applicability to various geometries including planar, disk, ring and cylindrical structures, and the ability to induce and control motion of passive shafts remotely. They can also achieve higher speed. Their power efficiency is less than 50%, due to the requirement for two

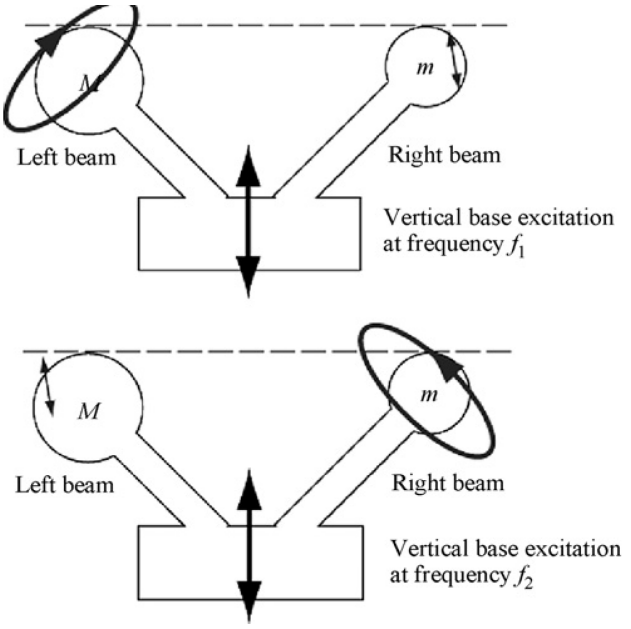

FIGURE 20. The dual fin device by Friend *et al.* [82] ©2006 IEEE.

vibration waves, which is considerable lower than the 80% or more that can be achieved by standing wave motors [34].

In practice, the natural vibration modes of the stator are employed, because of the high vibration amplitude that is achieved. A traveling wave can also be achieved by one vibration source and a vibration receiver, both in contact to the stator. The receiver is not electrically powered but its resistance can be adjusted to achieve a traveling wave along the vibration travelling medium. In this way, a shaft in contact with the stator can be propelled. Various other ultrasonic motor implementations have been reported. Applications include camera lens motion, watch mechanisms, smart-phone integrated optical zooms, micro-moving and micro-flying robots, precision positioning, and aerospace mechanisms. The ultrasonic motor principle has also been used to propel nanomotors. In [83], ultrasound waves have been used to propel nano-capsules for drug delivery applications, using an additional magnetic field for steering. Another remotely actuated crawling robot was presented in [84], In that system, magnetically induced vibration is used to propel a 1 mm diameter biomedical robot inside vessels and other cavities. More information about ultrasonic motors and their applications can be found in [85]. In parallel to the wave dynamics, key important technologies for such systems include friction engineering, and the optimization of mechanically pre-loading the motion interfaces with a permanent force.

Other micro-motor types include the hula-hoop or wobble motor mentioned in Section V.B. Various promising piezoelectric [34], electrostatic [78], [86] and electromagnetic [87] implementations can be found in the literature. A more detailed introduction to micro-walking devices and ultrasonic motors can be found in the reviews by Peng *et al* [81], Takeshi Morita [88], Watson *et al* [89], Zhao [85] and Uchino [34]. Pedagogical animations of various piezoelectric motion concepts are also available from Physik Instrumente [90].

B. RESONANCE

In the case of periodic motion, it is possible to obtain motion amplification by exploitation of resonance. If, for example, a tip is stimulated externally at its natural frequency, each motion phase contributes energy to the tip. Provided that the added energy is larger than that removed by damping, it increases the vibration amplitude. The maximum motion amplification that is obtained is equal to the oscillator quality factor Q:

$$g = Q = \frac{1}{2\zeta}$$

where ζ is the damping ratio. This type of motion amplification is not applicable to quasi-static operation systems such as micro-grippers, but can be very practical for microsystems with fast repeatable motions such as micro-scanners and micro-motors. For example, a micro-scanner with motion amplification of over 70 at 440 Hz, used as a scanner in a magnetic resonance elastography system, was reported in [91]. Resonance can also be used in combination with other motion amplifiers and structures that translate linear motion to other directions or to rotation [92].

Motion amplification can also be achieved by parametric resonance, i.e. resonance that is indirectly induced by modulating a parameter of the oscillating system, for example by a perpendicular motion source. Example systems include a proof mass modulation based torsion spring system for watch applications [93], and a gyroscope with increased internal motion range for higher signal to noise ratio [94].

Typical applications of resonance-based motion amplification include atomic force microscopy [95] and other nanopositioning systems that involve scanning, such as the ion-conductance microscopy XYZ stage presented in [96]. Furthermore, in mirror scanners for displays, synchronous rotational oscillation of micro-mirrors is desirable at high angle and frequency. This motion range can be directly achieved electrostatically or electromagnetically, but piezoelectric implementations are especially attractive for compact, integrated and low power devices. The small displacement of thin film piezoelectrics can be amplified by mechanical resonance at a frequency that is suitable for scanning. For example, in [97], a rotational angle range of 38.5º for a 1.4 mm wide mirror is obtained by resonance, using a 24 V, 40 kHz driving voltage. Resonance motion amplification is also used in electromagnetic micro-mirror arrays to enhance the angle range, as in [98], where horizontal and vertical scanning with angle range of 36° at 21 kHz and 18° at 60 Hz is achieved using a Ø 1.2 mm mirror.

Structures for motion amplification by resonance are also used in energy harvesting devices to obtain a large internal displacement from small amplitude vibrations.

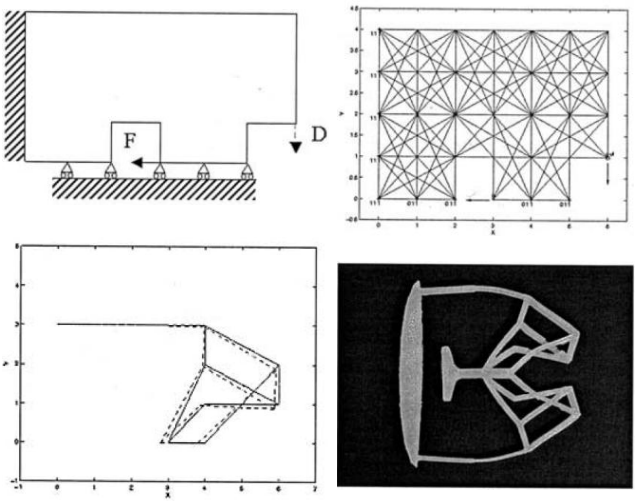

FIGURE 21. A two-dimensional example of compliant mechanism design. Top-left: The initial design space and input/output specification. Top-right: Initial guess of a beam network. Bottom-left: Optimization of network using numerical simulation. Bottom-right: Optimized compliant mechanism. By Kota *et al.* [105] ©Springer. Reproduced with permission.

Direct and parametric resonance have both been studied in various transducer types and geometries, and for various motion sources [99], [100]. Introductions and reviews on motion energy harvesting can be found in [41], [42].

Resonance mechanical amplification is used also in acoustic speakers and horn structures, but the resulting acoustic vibration output is in the form of sound rather than mass motion. This type of motion amplifier lies beyond the scope of this review. For some interesting loudspeaker implementations, the reader is referred to the acoustical patent review of Fulop and Rice [101].

Beyond the various structure types and design methods for motion amplification that have been discussed in this section, the field of compliant mechanisms provides a more holistic approach for optimized motion translation systems. This approach is reviewed in the next section of this paper.

VII. COMPLIANT MECHANISMS

A special method of developing systems with motion amplification is the concept of designing compliant mechanisms. The concept of compliant mechanisms offers a systematic method of optimizing a monolithic design to achieve a given desired geometrical or mechanical advantage within specified constraints. Although not fully researched and exploited, this method is currently the most developed among motion amplification technologies.

The design approach of compliant mechanisms is based on seeking a monolithic geometry of a material with given mechanical properties that provides the desirable transfer function while optimizing one or more functional parameters of the system. Such parameters include size, shape, energy transfer efficiency, reliability, endurance and resonance modes. As an example, a two-dimensional design case is described in Fig. 21. The design can comprise a network of beams of selectable and varying cross sections, including flexure joints. The possible combinations are evaluated by numerical simulations against the optimization criteria, sequentially or by using a prediction and selection algorithm. The optimization can be performed either in a single stage, or in multiple stages through which the first stage design is refined. Early examples of compliant mechanisms are the optimized hand-tool of Howell and Midha [102] and the negative-Poisson's ratio metamaterial of Larsen *et al.* [103]. Efforts for integrating compliant mechanisms in energy harvesting devices for low frequency, large amplitude motion have also been reported [104].

A multistage optimization method for designing compliant mechanisms has been developed by Howell and Midha [102]. In this method, a topology synthesis with an initial pseudo-rigid-body analysis is performed, by including rigid beams, flexural joints and flexible beams in an initial geometrical arrangement. The behavior of flexible beams is modelled as torsional springs at rigid-body joints. This analysis results in a first design with defined rigid links and joints, which gives the desirable force and displacement translation. In the second stage, the topology is modified to improve performance in terms of mechanical / geometrical advantage, size, shape and energy efficiency [105], within a given set of system constraints, such as size or stress limits. Design variables include the length of rigid beams and the elasticity of the joints [102]. In a third stage, the behavior of the full compliant system is studied by finite element modelling. This can be done by discretization of the monolithic structure into elementary parts and successive analysis of each element as a beam [102], with additional boundary conditions where needed. If further room for improvement is identified, the first or second stage design can be modified and re-evaluated, allowing fine-tuning of the system response. A dynamic response analysis may also be included for performance evaluation in systems involving resonant or dynamic environments or functionality [106].

An overview of compliant mechanism technology, including synthesis methods and example microelectromechanical systems, is available in the textbook of Howell *et al.* [107]. Furthermore, a comprehensive overview of flexure-based compliant mechanisms has been published by Lobontiu [62]. Other topology optimization techniques could also be employed for compliant systems. In the general field of topology optimization, a material distribution function that minimizes a set of optimization parameters under given constraints is sought. This research field was rapidly developed in the previous two decades, introducing various new approaches, including density-based methods, evolutionary structural optimization, and boundary variation methods [108]. A bio-inspired method was also introduced which is based on structural evolution mimicking the process of cell division. Such a method was employed for the aeroelastic optimization of flapping membranes for micro air vehicles [109]. For an overview of topology optimization methods the reader is referred to the reviews of Sigmund and Maute [110], and of Deaton and Grandhi [108].

TABLE 2. Summary of motion amplification mechanisms.

Mechanism	*Direct Leverage*	*V-shaped Beam*	*Unimorph*	*Flextensional*	*Scott-Russel*	*Micro-Walking*	*Resonance*
Theoretical gain	$\frac{L_2}{L_1}$	$cot\theta_1$, $sin^{-1}\theta_1$	$\theta = \frac{\Delta L}{b}$ $\Delta y = \frac{L}{\theta} \cdot (1 - cos\theta)$	$cot\theta_1$	$cot\theta_1$	∞	Q
State-of-art gain	10 [20]	10 [20]	80 [36]	40 [45]	6 [75]	∞	70 [91]
Main Actuation mechanisms	Piezoelectric, Electrostatic	Electothermal Piezoelectric	Piezoelectric Electrothermal	Piezoelectric	Piezoelectric	Piezoelectric	Piezoelectric Electromagnetic
Fabrication methods	MEMS	MEMS	MEMS	MEMS Lamination	MEMS	MEMS	MEMS
Main Applications	Micromirror Displays Microgrippers	Microgrippers Nanoposition	Energy Harvesting Sensors	Actuation Microgrippers Nanoposition	Microgrippers Nanoposition	Micromotors Nanoposition	AFM, Micromirror Displays Energy Harvesting
References	[12-20]	[20-22, 24-33]	[36-43]	[3, 21, 22, 29, 44-71]	[72-77]	[34, 79, 81, 82, 85, 88-90]	[41, 42, 91-101]

In conclusion, the maturity of compliant mechanism design technology offers a valuable tool for the development of MEMS with amplified motion range. The advanced analytical and numerical methods allow synthesis and evaluation of novel designs customized to application requirements. The combination of corresponding simulation software, 3D printing and MEMS fabrication can allow rapid prototyping of novel actuation, sensing and micro-energy systems in the mm to μm scale. The wide availability of these tools can be expected to drive a rapid development in the fields of micro-robotics, energy harvesting devices and medical microsystems within the next five years. Opportunities in this roadmap include the combination of compliant mechanisms with advanced nano-materials, the incorporation of advanced compliant joint technology [111] in the design analysis, and the integration of active materials into compliant structures, which is expected to unlock a new range of micro motion devices. The development of numerical simulation software that combines strain and kinematic modeling is highly desirable in model evaluation, accurate prediction of performance, structural optimization, and functionality visualization of compliant mechanisms and other motion amplification structures. Towards this direction, computational tools implementing compliant mechanism design algorithms have been proposed [112]–[114].

VIII. CONCLUSION AND OUTLOOK

The direct displacement that can be provided by state-of-the-art active materials and microstructures is in the range of 0.1% of the material size, for reasonable actuating field or temperature range values. Therefore, motion amplification mechanisms are required in order to enable actuating functionality up to the millimeter scale, where electromagnetic actuation is not favorable due to flux availability limitations. In this direction, the development and integration of higher strain materials, especially elastomers [115], [116], comprise a very promising research area.

Direct or indirect leverage is commonly used to achieve micromotion amplification, both in piezoelectric, electrostatic or electrothermal systems. Simple considerations show that the geometrical gain available is typically in the range of the structural aspect ratio that can be achieved. The employment of flexural joints leads to high performance because flexures allow the application of input displacements in the close vicinity of an effective pivotal point. Additional advantages include fabrication simplicity and the ability of using multiple flexures on a single monolithic structure. The motion amplification principle of unimorphs can also be considered as a type of leverage, with the geometrical gain being determined by the depth of the zero-stress plane in a beam compared with the beam length. This depends on the bending stiffness of the materials used. Finally, dynamic motion amplification can be achieved either by implementing a fast, repeatable motion cycle, such as in micro-walking devices, or by resonance, where an oscillating structure can accumulate mechanical energy over time.

A summary of the various motion amplification mechanisms that have been studied and reviewed is presented in Table 2. The table includes the theoretically expected motion amplification as well as the values that are typically achieved from single-stage implementations in the current state-of-art. Each leverage stage typically provides an amplification gain of 10. Multi-flexure flextensional mechanisms with gains as high as 40 are currently available, with the output stroke approaching 1% of the device size. Unimorph structures provide gains as high as 80 by employing thin films to achieve a high length to zero-stress depth aspect ratio. Micro-walking structures and micromotors provide a practically infinite motion range. Oscillator structures can provide a motion amplification equal to their quality factor and demonstrated values up to 80 have been reported.

These two dynamic approaches find very important applications in cases where repetitive motion (e.g. micro-mirror systems) or a long traveling range (e.g. precision positioning) is required.

The combination of microscale, active elements with structures implementing multiple stage motion amplification is a very promising approach for integrated microsystems that need to interact in the macroscale environment, indicatively at sizes above 1 mm. The employment of the compliant mechanisms methodology can offer systematic design and is expected to yield optimized interactive sensor and actuator systems. In turn, such systems could provide additional functionality, improved compactness and simplicity to current micromotor – based millimeter scale robotics.

The combination of high-force piezoelectric beam elements with compliant designs is of special interest because it could provide large travelling or rotating range for applications not requiring a high force. The availability of a wide range of high-performance piezoelectric beams as single components and the accessibility of high resolution 3D printing for various materials provide a simple and low-cost method for rapid prototyping and testing new ideas. These could be combined with advanced manufacturing methods for flexible substrates that have emerged in recent years including flexures. An example can be found in the advanced lamination-based flexure fabrication methods developed at the Harvard Microrobotics Lab. Various motion amplification methods have been implemented by these methods, enabling promising microsystems such as insect-scale robots [117], [118]. It is expected that based on this state-of-art, various bespoke, millimeter scale actuator systems offering amplified motion for specific applications will emerge in the coming years. For this purpose, the availability of simulation software with the capability of fast calculation of kinetics and compliance of structures in 3D would be highly desirable. Such software is not currently widely available. Some computational tools with optimization capability can be found in [112]–[114].

The implementation of motion amplification concepts is also beneficial for systems actively operating in the microscale, such as microgrippers and microvalves. As an example, the microgripper reported in [119] employs direct leverage to provide a passive gripping action. The integration of such structures with active materials and other motion amplification structures is expected to expand the capability of state-of-art microsystems. This would directly benefit application fields of wide importance such as microscale vehicles, biomedical fibre robotics and micro-robotics for surgery.

3D nanoscale lithography technologies are expected to play a major role in implementing motion amplification techniques in microscale systems. The emergence and rapid development of the two-photon polymerization (2PP) in the last two decades [120], [121] has already enabled the fabrication of advanced functional microstructures at sizes as low as 10 μm. As an example, an SEM image of the microgripper system fabricated by Power *et al* using 2PP technology is shown in Fig. 22 [119]. Utilizing this technology for other materials including metals, by fusion of metal nanoparticles embedded in the photoresist polymers [122], and its combination with other microfabrication methods such as LIGA (Lithographie, Galvanoformung, Abformung), is expected to enable a new class of motion-amplification based microscale actuators in the near future.

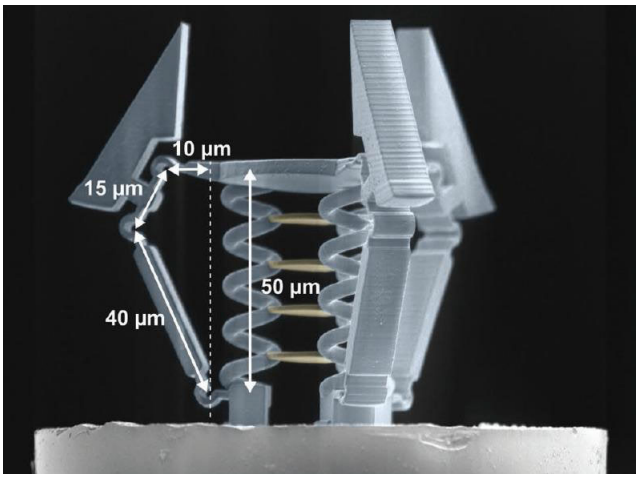

FIGURE 22. SEM image of a microgripper fabricated on the tip of a Ø 125 μm optical fiber using two photon photopolymerization 3D lithography, by Power *et al.* [119]. ©Wiley. Reproduced with permission.

Overall, various new actuation methods have been investigated and demonstrated in the lab, some of which are very promising for future applications. However, the combination of conventional piezoelectric, electrostatic and electrothermal actuation methods with motion amplification structures offers a systematic and reliable design space for addressing the micromotion requirements of a large range of applications. Therefore, motion amplification systems are expected to play a central role in the enabling of millimeter and micrometer scale actuating, robotic, sensing as well as energy systems. The classification and study presented in this paper provides an overview, which may assist the development and employment of new motion amplification mechanisms in applications requiring microscale motion.

REFERENCES

[1] APC International Ltd. (2017). *Physical and Piezoelectric Properties of APC Materials*. [Online]. Available: https://www.americanpiezo.com/apc-materials/piezoelectric-properties.html

[2] Chicago Telephone Supply (CTS) Corporation. (2016). *Piezoelectric PMN-PT Single Crystal Products*. [Online]. Available: www.ctscorp.com/wp-content/uploads/2016.12.15-Single-Crystal-Brochure.pdf

[3] P. A. York, N. T. Jafferis, and R. J. Wood, "Meso scale flextensional piezoelectric actuators," *Smart Mater. Struct.*, vol. 27, no. 1, Jan. 2018, Art. no. 015008.

[4] Cedrat Technologies. (2018). *Multilayer Actuators MLA Series, Products Catalog Version 4.1*. [Online]. Available: www.cedrat-technologies.com/download/CEDRAT_TEC_Catalogue.pdf

[5] C. Livermore. (2007). *Design and Fabrication of Microelectromechanical Devices*. [Online]. Available: http://ocw.mit.edu/

[6] W.-M. Zhang, H. Yan, Z.-K. Peng, and G. Meng, "Electrostatic pull-in instability in MEMS/NEMS: A review," *Sens. Actuators A, Phys.*, vol. 214, pp. 187–218, Aug. 2014.

[7] J. Felder, E. Lee, and D. L. DeVoe, "Large vertical displacement electrostatic zipper microstage actuators," *J. Microelectromech. Syst.*, vol. 24, no. 4, pp. 896–903, Aug. 2015.

[8] F. Heibeck, B. Tome, C. D. Silva, and H. Ishii, "uniMorph: Fabricating thin film composites for shape-changing interfaces," in *Proc. 28th Annu. ACM Symp. User Interface Softw. Technol. UIST*, Charlotte, NC, USA, 2015, pp. 233–242.

[9] X. Zhang, Z. Yu, C. Wang, D. Zarrouk, J.-W.-T. Seo, J. C. Cheng, A. D. Buchan, K. Takei, Y. Zhao, J. W. Ager, J. Zhang, M. Hettick, M. C. Hersam, A. P. Pisano, R. S. Fearing, and A. Javey, "Photoactuators and motors based on carbon nanotubes with selective chirality distributions," *Nature Commun.*, vol. 5, no. 1, p. 2983, May 2014.

[10] L. Hines, K. Petersen, G. Z. Lum, and M. Sitti, "Soft actuators for small-scale robotics," *Adv. Mater.*, vol. 29, no. 13, Apr. 2017, Art. no. 1603483.

[11] T. Khudiyev, J. Clayton, E. Levy, N. Chocat, A. Gumennik, A. M. Stolyarov, J. Joannopoulos, and Y. Fink, "Electrostrictive microelectromechanical fibres and textiles," *Nature Commun.*, vol. 8, no. 1, p. 1435, Dec. 2017.

[12] C. Bolzmacher, K. Bauer, U. Schmid, M. Hafez, and H. Seidel, "Displacement amplification of piezoelectric microactuators with a micromachined leverage unit," *Sens. Actuators A, Phys.*, vol. 157, no. 1, pp. 61–67, Jan. 2010.

[13] S. Rajgopal, A. Knobloch, S. Kennerly, and M. Mehregany, "A piezoelectrically-actuated valve for modulation of liquid at high flow rate under high pressure," in *Proc. TRANSDUCERS Int. Solid-State Sensors, Actuat. Microsyst. Conf.*, vol. 1, Jun. 2007, pp. 743–746.

[14] H. S. Fiaz, C. R. Settle, and K. Hoshino, "Metal additive manufacturing for microelectromechanical systems: Titanium alloy (Ti-6Al-4 V)-based nanopositioning flexure fabricated by electron beam melting," *Sens. Actuators A, Phys.*, vol. 249, pp. 284–293, Oct. 2016.

[15] J.-C. Tsai and M. C. Wu, "Design, fabrication, and characterization of a high fill-factor, large scan-angle, two-axis scanner array driven by a leverage mechanism," *J. Microelectromech. Syst.*, vol. 15, no. 5, pp. 1209–1213, Oct. 2006.

[16] H. Ren, F. Tao, W. Wang, and J. Yao, "An out-of-plane electrostatic actuator based on the lever principle," *J. Micromech. Microeng.*, vol. 21, no. 4, Apr. 2011, Art. no. 045019.

[17] S. Yang, Q. Xu, and Z. Nan, "Design and development of a dual-axis force sensing MEMS microgripper," *J. Mech. Robot.*, vol. 9, no. 6, Dec. 2017, Art. no. 061011.

[18] C.-H. Han, D.-H. Choi, H.-H. Yang, Y.-H. Yoon, and J.-B. Yoon, "Voltage-controlled $C-V$ response tuning in a parallel plate MEMS variable capacitor," *J. Microelectromech. Syst.*, vol. 22, no. 6, pp. 1403–1413, Dec. 2013.

[19] Y.-H. Song, C.-H. Han, M.-W. Kim, J. O. Lee, and J.-B. Yoon, "High-performance MEMS relay using a stacked-electrode structure and a levering and torsional spring for power applications," in *Proc. IEEE 25th Int. Conf. Micro Electro Mech. Syst. (MEMS)*, Jan. 2012, pp. 84–87.

[20] H. Steiner, W. Hortschitz, M. Stifter, F. Keplinger, and T. Sauter, "Thermal actuators featuring large displacements for passive temperature sensing," *Microsyst. Technol.*, vol. 20, nos. 4–5, pp. 551–557, Apr. 2014.

[21] M. Ling, J. Cao, M. Zeng, J. Lin, and D. J. Inman, "Enhanced mathematical modeling of the displacement amplification ratio for piezoelectric compliant mechanisms," *Smart Mater. Struct.*, vol. 25, no. 7, Jul. 2016, Art. no. 075022.

[22] C. Liang, F. Wang, B. Shi, Z. Huo, K. Zhou, Y. Tian, and D. Zhang, "Design and control of a novel asymmetrical piezoelectric actuated microgripper for micromanipulation," *Sens. Actuators A, Phys.*, vol. 269, pp. 227–237, Jan. 2018.

[23] E. Davies, D. S. George, M. C. Gower, and A. S. Holmes, "MEMS Fabry-Pérot optical accelerometer employing mechanical amplification via a V-beam structure," *Sens. Actuators A, Phys.*, vol. 215, pp. 22–29, Aug. 2014.

[24] M. J. Sinclair, "A high force low area MEMS thermal actuator," in *Proc. ITHERM 7th Intersociety Conf. Thermal Thermomechanical Phenomena Electron. Syst.*, vol. 1, May 2000, pp. 127–132.

[25] J. J. Brown and V. M. Bright, "Thermal Actuators," in *Encyclopedia of Nanotechnology*, B. Bhushan, Ed. Dordrecht, The Netherlands: Springer, 2012, pp. 2680–2697.

[26] Nanofabrication Laboratory, University of Utah. (2018). *Scaling Principles*. [Online]. Available: https://www.nanofab.utah.edu/cool-stuff/

[27] K. Kwack and K. Chun, "Very high displacement to voltage ratio MEMS thermal actuator," *IEEE Sensors*, Busan, South Korea, Nov. 2015, pp. 1–4.

[28] S. Bergna, J. J. Gorman, and N. G. Dagalakis, "Design and modeling of thermally actuated MEMS nanopositioners," in *Proc. Int. Mech. Eng. Congr. Expo. (IMECE)*, Jan. 2005, pp. 561–568.

[29] Y.-S. Kim, H. Shi, N. G. Dagalakis, and S. K. Gupta, "Design of a MEMS-based motion stage based on a lever mechanism for generating large displacements and forces," *J. Micromech. Microeng.*, vol. 26, no. 9, Sep. 2016, Art. no. 095008.

[30] H. L. Shi, Y. Kim, and Y. She, "Design of a Parallel Kinematic MEMS XY Nanopositioner," in *Proc. IEEE Int. Conf. Robot. Biomimetics (ROBIO)*, Dec. 2015, pp. 1973–1978.

[31] C. Lee and C.-Y. Wu, "Study of electrothermal V-beam actuators and latched mechanism for optical switch," *J. Micromech. Microeng.*, vol. 15, no. 1, pp. 11–19, Jan. 2005.

[32] H.-W. Huang, F.-W. Lee, and Y.-J.-J. Yang, "Design criteria for a push-on push-off MEMS bistable device," *J. Microelectromech. Syst.*, vol. 25, no. 5, pp. 900–908, Oct. 2016.

[33] H. Steiner, M. Stifter, W. Hortschitz, and F. Keplinger, "Planar magnetostrictive micromechanical actuator," *IEEE Trans. Magn.*, vol. 51, no. 1, pp. 1–4, Jan. 2015.

[34] K. Uchino, "Piezoelectric ultrasonic motors: Overview," *Smart Mater. Struct.*, vol. 7, no. 3, pp. 273–285, Jun. 1998.

[35] S. Timoshenko, "Analysis of bi-metal thermostats," *J. Opt. Soc. Amer.*, vol. 11, no. 3, p. 233, Sep. 1925.

[36] J. S. Pulskamp, R. G. Polcawich, R. Q. Rudy, S. S. Bedair, R. M. Proie, T. Ivanov, and G. L. Smith, "Piezoelectric PZT MEMS technologies for small-scale robotics and RF applications," *MRS Bull.*, vol. 37, no. 11, pp. 1062–1070, Nov. 2012.

[37] R. Seveno, B. Guiffard, and J.-P. Regoin, "Ultra large deflection of thin PZT/aluminium cantilever beam," *Funct. Mater. Lett.*, vol. 8, no. 5, Oct. 2015, Art. no. 1550051.

[38] Omega Piezo. (2018). *Strip Actuators*. [Online]. Available: http://www.omegapiezo.com/strip-actuators-bimorph-equivalent/

[39] H. Conrad, H. Schenk, B. Kaiser, S. Langa, M. Gaudet, K. Schimmanz, M. Stolz, and M. Lenz, "A small-gap electrostatic micro-actuator for large deflections," *Nature Commun.*, vol. 6, no. 1, p. 10078, Dec. 2015.

[40] A. Erturk and D. J. Inman, *Piezoelectric Energy Harvesting*. Chichester, U.K.: Wiley, 2011.

[41] S. Roundy, P. K. Wright, and J. Rabaey, "A study of low level vibrations as a power source for wireless sensor nodes," *Comput. Commun.*, vol. 26, no. 11, pp. 1131–1144, Jul. 2003.

[42] P. D. Mitcheson, E. M. Yeatman, G. K. Rao, A. S. Holmes, and T. C. Green, "Energy harvesting from human and machine motion for wireless electronic devices," *Proc. IEEE*, vol. 96, no. 9, pp. 1457–1486, Sep. 2008.

[43] M. E. Kiziroglou and E. M. Yeatman, "Materials and techniques for energy harvesting," in *Functional Materials for Sustainable Energy Applications*, E. Kilner, Ed. Sawston, U.K.: Woodhead Publishing, 2012.

[44] J. H. Kim, S. H. Kim, and Y. K. Kwak, "Development and optimization of 3-D bridge-type hinge mechanisms," *Sens. Actuators A, Phys.*, vol. 116, no. 3, pp. 530–538, Oct. 2004.

[45] F. Chen, Z.-J. Du, M. Yang, F. Gao, W. Dong, and D. Zhang, "Design and analysis of a three-dimensional bridge-type mechanism based on the stiffness distribution," *Precis. Eng.*, vol. 51, pp. 48–58, Jan. 2018.

[46] W. Dong, F. Chen, M. Yang, Z.-J. Du, J. Tang, and D. Zhang, "Development of a highly efficient bridge-type mechanism based on negative stiffness," *Smart Mater. Struct.*, vol. 26, no. 9, Sep. 2017, Art. no. 095053.

[47] L.-J. Lai and Z.-N. Zhu, "Design, modeling and testing of a novel flexure-based displacement amplification mechanism," *Sens. Actuators A, Phys.*, vol. 266, pp. 122–129, Oct. 2017.

[48] Y. Li and Q. Xu, "A novel piezoactuated XY stage with parallel, decoupled, and stacked flexure structure for micro-/Nanopositioning," *IEEE Trans. Ind. Electron.*, vol. 58, no. 8, pp. 3601–3615, Aug. 2011.

[49] J. Park, H. Lee, H. Kim, H. Kim, and D. Gweon, "Note: Development of a compact aperture-type XYz positioning stage," *Rev. Sci. Instrum.*, vol. 87, no. 3, Mar. 2016, Art. no. 036112.

[50] X. Zhang, Y. Zhang, and Q. Xu, "Design and control of a novel piezo-driven XY parallel nanopositioning stage," *Microsyst. Technol.*, vol. 23, no. 4, pp. 1067–1080, Apr. 2017.

[51] C. Liang, F. Wang, Y. Tian, and D. Zhang, "Design and modeling of a 2-DOF decoupled rotation platform for micro-manipulation," in *Proc. IEEE Int. Conf. Manipulation, Manuf. Meas. Nanosc. (3M-NANO)*, Aug. 2017, pp. 7–12.
[52] F. Wang, C. Liang, Y. Tian, X. Zhao, and D. Zhang, "Design and characteristics of a compliant microgripper dedicated to fast microhandling," in *Proc. Int. Conf. Manipulation, Manuf. Meas. Nanosc. (3M-NANO)*, Oct. 2015, pp. 79–84.
[53] Y.-L. Yang, Y.-D. Wei, J.-Q. Lou, F.-R. Xie, and L. Fu, "Development and precision position/force control of a new flexure-based microgripper," *J. Micromech. Microeng.*, vol. 26, no. 1, Jan. 2016, Art. no. 015005.
[54] K.-Q. Qi, Y. Xiang, C. Fang, Y. Zhang, and C.-S. Yu, "Analysis of the displacement amplification ratio of bridge-type mechanism," *Mechanism Mach. Theory*, vol. 87, pp. 45–56, May 2015.
[55] H.-W. Ma, S.-M. Yao, L.-Q. Wang, and Z. Zhong, "Analysis of the displacement amplification ratio of bridge-type flexure hinge," *Sens. Actuators A, Phys.*, vol. 132, no. 2, pp. 730–736, Nov. 2006.
[56] L. Ma, Z. F. He, and H. K. Ouyang, "Analysis of Bridge-type Nano-positioning Stage," in *Frontiers of Manufacturing and Design Science* (Applied Mechanics and Material), vols. 44–47, R. Chen, Ed. Bäch, Switzerland: Trans Tech Publications Ltd, 2011, pp. 3828–3832.
[57] K.-B. Choi, J. J. Lee, G. H. Kim, H. J. Lim, and S. G. Kwon, "Amplification ratio analysis of a bridge-type mechanical amplification mechanism based on a fully compliant model," *Mechanism Mach. Theory*, vol. 121, pp. 355–372, Mar. 2018.
[58] L. Clark, B. Shirinzadeh, J. Pinskier, Y. Tian, and D. Zhang, "Topology optimisation of bridge input structures with maximal amplification for design of flexure mechanisms," *Mechanism Mach. Theory*, vol. 122, pp. 113–131, Apr. 2018.
[59] C. Lin, Z. Shen, Z. Wu, and J. Yu, "Kinematic characteristic analysis of a Micro-/Nano positioning stage based on bridge-type amplifier," *Sens. Actuators A, Phys.*, vol. 271, pp. 230–242, Mar. 2018.
[60] J. Wang and X. Liu, "Generalized equations for estimating stress concentration factors of various notch flexure hinges," *J. Mech. Design*, vol. 136, no. 3, Mar. 2014, Art. no. 031009.
[61] P. Liu and P. Yan, "A new model analysis approach for bridge-type amplifiers supporting Nano-stage design," *Mechanism Mach. Theory*, vol. 99, pp. 176–188, May 2016.
[62] N. Lobontiu, "Compliant mechanisms," in *Design of Flexure Hinges*. Boca Raton, FL, USA: CRC Press, 2002.
[63] N. Lobontiu and E. Garcia, "Analytical model of displacement amplification and stiffness optimization for a class of flexure-based compliant mechanisms," *Comput. Struct.*, vol. 81, no. 32, pp. 2797–2810, Dec. 2003.
[64] Cedrat Technologies. (2018). *Amplified Piezoelectric Actuators*. [Online]. Available: www.cedrat-technologies.com/en/products/actuators/apa.html
[65] PiezoDrive. (2018). *AP Series Amplified Piezoelectric Actuators*. [Online]. Available: www.piezodrive.com/actuators/ap-series-amplified-piezoelectric-actuators/
[66] Thorlabs Inc. (2018). *Amplified Piezoelectric Actuators, 220 μm to 1500 μm Travel*. Available:. [Online]. Available: www.thorlabs.com/newgrouppage9.cfm?objectgroup_id=8700&pn=PK2FVF1
[67] QorTek. (2018). *TITAN Amplified Piezoelectric Actuator Products*. [Online]. Available: www.qortek.com/en/products/actuators/titan-amplified-piezoelectric-actuators/
[68] Dynamic Structures and Materials LLC. (2018). *Flextensional Piezo Actuators (FPA) Series*. [Online]. Available: www.dynamic-structures.com/actuators#fpa
[69] Noliac. (2018). *Amplified actuators*. [Online]. Available: www.noliac.com/products/actuators/amplified-actuators/
[70] PI (Physik Instrumente) LP. (2018). *Introduction to Flexure-Guided and Motion-Amplified Piezo Actuators*. [Online]. Available: www.pi-usa.us/products/PiezoActuators/index.php#FLEXURE
[71] Dynamic Structures and Materials LLC. (2018). *Lever-Amplified Flextensional Piezo Actuators (LFPA) Series*. [Online]. Available: https://www.dynamic-structures.com/wp-content/uploads/2018/04/LFPA-10000-1072.pdf
[72] Y. Liu and Q. Xu, "Mechanical design, analysis and testing of a large-range compliant microgripper," *Mech. Sci.*, vol. 7, no. 1, pp. 119–126, 2016.
[73] J.-L. Ha, Y.-S. Kung, S.-C. Hu, and R.-F. Fung, "Optimal design of a micro-positioning scott-russell mechanism by taguchi method," *Sens. Actuators A, Phys.*, vol. 125, no. 2, pp. 565–572, Jan. 2006.
[74] C.-M. Chen, Y.-C. Hsu, and R.-F. Fung, "System identification of a Scott–Russell amplifying mechanism with offset driven by a piezoelectric actuator," *Appl. Math. Model.*, vol. 36, no. 6, pp. 2788–2802, Jun. 2012.
[75] W.-L. Zhu, Z. Zhu, P. Guo, and B.-F. Ju, "A novel hybrid actuation mechanism based XY nanopositioning stage with totally decoupled kinematics," *Mech. Syst. Signal Process.*, vol. 99, pp. 747–759, Jan. 2018.
[76] G. Y. Liao, "Design and analysis of a modified scott russell straight-line mechanism for a robot end-effector," *J. Appl. Sci. Eng. Technol.*, vol. 4, pp. 42–49, Sep. 2011.
[77] X. Sun, W. Chen, Y. Tian, S. Fatikow, R. Zhou, J. Zhang, and M. Mikczinski, "A novel flexure-based microgripper with double amplification mechanisms for micro/nano manipulation," *Rev. Sci. Instrum.*, vol. 84, no. 8, Aug. 2013, Art. no. 085002.
[78] D. K.-C. Liu, J. Friend, and L. Yeo, "A brief review of actuation at the micro-scale using electrostatics, electromagnetics and piezoelectric ultrasonics," *Acoust. Sci. Technol.*, vol. 31, no. 2, pp. 115–123, 2010.
[79] T. Hu, Y. Zhao, X. Li, Y. Zhao, and Y. Bai, "Design and fabrication of an electro-thermal linear motor with large output force and displacement," in *Proc. IEEE Sensors*, Oct. 2016, pp. 1–3.
[80] J. Kedzierski and E. Holihan, "Linear and rotational microhydraulic actuators driven by electrowetting," *Sci. Robot.*, vol. 3, no. 22, Sep. 2018, Art. no. eaat5643.
[81] Y. Peng, Y. Peng, X. Gu, J. Wang, and H. Yu, "A review of long range piezoelectric motors using frequency leveraged method," *Sens. Actuators A, Phys.*, vol. 235, pp. 240–255, Nov. 2015.
[82] J. Friend, Y. Gouda, K. Nakamura, and S. Ueha, "A simple bidirectional linear microactuator for nanopositioning–the 'Baltan' microactuator," *IEEE Trans. Ultrason., Ferroelectr., Freq. Control*, vol. 53, no. 6, pp. 1160–1168, Jun. 2006.
[83] V. Garcia-Gradilla, J. Orozco, S. Sattayasamitsathit, F. Soto, F. Kuralay, A. Pourazary, A. Katzenberg, W. Gao, Y. Shen, and J. Wang, "Functionalized ultrasound-propelled magnetically guided nanomotors: Toward practical biomedical applications," *ACS Nano*, vol. 7, no. 10, pp. 9232–9240, Oct. 2013.
[84] M. Medical. (Dec. 5, 2018). *ViRob Platform*. [Online]. Available: http://www.microbotmedical.com/technology/virob/
[85] C. Zhao, "Ultrasonic motors," *Technologies and Applications*. Berlin, Germany: Springer-Verlag, 2011.
[86] S. Pranonsatit, G. Hong, A. S. Holmes, and S. Lucyszyn, "Rotary RF MEMS switch based on the wobble motor principle," in *19th IEEE Int. Conf. Micro Electro Mech. Syst.*, Jan. 2006, pp. 886–889.
[87] S. De Cristofaro, C. Stefanini, N. N. Pak, E. Susilo, M. C. Carrozza, and P. Dario, "Electromagnetic wobble micromotor for microrobots actuation," *Sens. Actuators A, Phys.*, vol. 161, nos. 1–2, pp. 234–244, Jun. 2010.
[88] T. Morita, "Miniature piezoelectric motors," *Sens. Actuators A, Phys.*, vol. 103, no. 3, pp. 291–300, Feb. 2003.
[89] B. Watson, J. Friend, and L. Yeo, "Piezoelectric ultrasonic micro/milliscale actuators," *Sens. Actuators A, Phys.*, vol. 152, no. 2, pp. 219–233, Jun. 2009.
[90] Physik Instrumente (PI). (Sep. 20, 2018). *Piezo Motors, Linear Motor Positioners & Rotary Piezo Motor Stages*. [Online]. Available: https://www.pi-usa.us/en/products/piezo-motors-stages-actuators/
[91] A. Arani, A. Eskandari, P. Ouyang, and R. Chopra, "A novel high amplitude piezoceramic actuator for applications in magnetic resonance elastography: A compliant mechanical amplifier approach," *Smart Mater. Struct.*, vol. 26, no. 8, Aug. 2017, Art. no. 087001.
[92] A. Ya'akobovitz, S. Krylov, and Y. Shacham-Diamand, "Large angle SOI tilting actuator with integrated motion transformer and amplifier," *Sens. Actuators A, Phys.*, vol. 148, no. 2, pp. 422–436, Dec. 2008.
[93] E. I. Butikov, "Parametric resonance in a linear oscillator at square-wave modulation," *Eur. J. Phys.*, vol. 26, no. 1, pp. 157–174, Jan. 2005.
[94] M. Sharma, E. H. Sarraf, R. Baskaran, and E. Cretu, "Parametric resonance: Amplification and damping in MEMS gyroscopes," *Sens. Actuators A, Phys.*, vol. 177, pp. 79–86, Apr. 2012.
[95] F. J. Giessibl, "Advances in atomic force microscopy," *Rev. Modern Phys.*, vol. 75, no. 3, pp. 949–983, Jul. 2003.
[96] S. Watanabe and T. Ando, "High-speed XYZ-nanopositioner for scanning ion conductance microscopy," *Appl. Phys. Lett.*, vol. 111, no. 11, Sep. 2017, Art. no. 113106.
[97] U. Baran, D. Brown, S. Holmstrom, D. Balma, W. O. Davis, P. Muralt, and H. Urey, "Resonant PZT MEMS scanner for high-resolution displays," *J. Microelectromech. Syst.*, vol. 21, no. 6, pp. 1303–1310, Dec. 2012.

[98] A. R. Cho, A. Han, S. Ju, H. Jeong, J.-H. Park, I. Kim, J.-U. Bu, and C.-H. Ji, "Electromagnetic biaxial microscanner with mechanical amplification at resonance," *Opt. Express*, vol. 23, no. 13, p. 16792, Jun. 2015.
[99] N. B. Caldwell and M. F. Daqaq, "Exploiting the principle parametric resonance of an electric oscillator for vibratory energy harvesting," *Appl. Phys. Lett.*, vol. 110, no. 9, Feb. 2017, Art. no. 093903.
[100] Y. Jia, J. Yan, K. Soga, and A. A. Seshia, "Multi-frequency operation of a MEMS vibration energy harvester by accessing five orders of parametric resonance," *J. Phys., Conf. Ser.*, vol. 476, no. 1, 2013, Art. no. 012126.
[101] S. A. Fulop and L. Rice, "Reviews of acoustical patents," *J. Acoust. Soc. Amer.*, vol. 142, no. 6, pp. 3347–3357, 2017.
[102] L. L. Howell and A. Midha, "A method for the design of compliant mechanisms with small-length flexural pivots," *J. Mech. Design*, vol. 116, no. 1, pp. 280–290, Mar. 1994.
[103] U. D. Larsen, O. Signund, and S. Bouwsta, "Design and fabrication of compliant micromechanisms and structures with negative Poisson's ratio," *J. Microelectromech. Syst.*, vol. 6, no. 2, pp. 99–106, Jun. 1997.
[104] X. Ma, A. Wilson, C. D. Rahn, and S. Trolier-McKinstry, "Efficient energy harvesting using piezoelectric compliant mechanisms: Theory and experiment," *J. Vibrat. Acoust.*, vol. 138, no. 2, Apr. 2016, Art. no. 021005.
[105] S. Kota, J. Joo, Z. Li, S. M. Rodgers, and J. Sniegowski, "Design of compliant mechanisms: Applications to MEMS," *Anal. Integr. Circuits Signal Process.*, vol. 29, no. 1, pp. 7–15, Oct. 2001.
[106] R. Agrawal, B. Shah, and E. Zimney, *Compliant Mechanisms and MEMS*. Evanston, IL, USA: Northwestern Univ., 2004.
[107] L. L. Howell, S. P. Magleby, and B. M. Olsen, *Handbook of Compliant Mechanisms*. Hoboken, NJ, USA: Wiley, 2013.
[108] J. D. Deaton and R. V. Grandhi, "A survey of structural and multidisciplinary continuum topology optimization: Post 2000," *Struct. Multidisciplinary Optim.*, vol. 49, no. 1, pp. 1–38, Jan. 2014.
[109] B. Stanford, P. Beran, and M. Kobayashi, "Aeroelastic optimization of flapping wing venation: A cellular division approach," *AIAA J.*, vol. 50, no. 4, pp. 938–951, Apr. 2012.
[110] O. Sigmund and K. Maute, "Topology optimization approaches," *Struct. Multidisciplinary Optim.*, vol. 48, no. 6, pp. 1031–1055, Dec. 2013.
[111] B. P. Trease, Y.-M. Moon, and S. Kota, "Design of large-displacement compliant joints," *J. Mech. Design*, vol. 127, no. 4, pp. 788–798, Jul. 2005.
[112] M. L. Culpepper and S. Kim, "A framework and design synthesis tool used to generate, evaluate and optimize compliant mechanism concepts for research and education activites," presented at the ASME Design Eng. Tech. Conf. Comput. Inf. Eng. Conf., Salt Lake, UT, USA, Oct. 2004.
[113] *Design Innovation and Simulation Laboratory (DISL)*. Accessed: Mar. 28, 2020. [Online]. Available: http://disl.osu.edu/
[114] V. Megaro, J. Zehnder, M. Bächer, S. Coros, M. Gross, and B. Thomaszewski, "A computational design tool for compliant mechanisms," *ACM Trans. Graph.*, vol. 36, no. 4, pp. 1–12, Jul. 2017.
[115] A. Miriyev, K. Stack, and H. Lipson, "Soft material for soft actuators," *Nature Commun.*, vol. 8, no. 1, p. 596, Dec. 2017.
[116] H. Zhao, A. M. Hussain, M. Duduta, D. M. Vogt, R. J. Wood, and D. R. Clarke, "Compact dielectric elastomer linear actuators," *Adv. Funct. Mater.*, vol. 28, no. 42, Oct. 2018, Art. no. 1804328.
[117] K. Y. Ma, P. Chirarattananon, and R. J. Wood, "Design and fabrication of an insect-scale flying robot for control autonomy," in *Proc. IEEE/RSJ Int. Conf. Intell. Robots Syst. (IROS)*, Sep. 2015, pp. 1558–1564.
[118] H. McClintock, F. Z. Temel, N. Doshi, J.-S. Koh, and R. J. Wood, "The milliDelta: A high-bandwidth, high-precision, millimeter-scale delta robot," *Sci. Robot.*, vol. 3, no. 14, Jan. 2018, Art. no. eaar3018.
[119] M. Power, A. J. Thompson, S. Anastasova, and G.-Z. Yang, "A monolithic force-sensitive 3D microgripper fabricated on the tip of an optical fiber using 2-Photon polymerization," *Small*, vol. 14, no. 16, Apr. 2018, Art. no. 1703964.
[120] S. Kawata, H.-B. Sun, T. Tanaka, and K. Takada, "Finer features for functional microdevices," *Nature*, vol. 412, no. 6848, pp. 697–698, Aug. 2001.
[121] S. Maruo, O. Nakamura, and S. Kawata, "Three-dimensional microfabrication with two-photon-absorbed photopolymerization," *Opt. Lett.*, vol. 22, no. 2, p. 132, Jan. 1997.
[122] A. Vyatskikh, S. Delalande, A. Kudo, X. Zhang, C. M. Portela, and J. R. Greer, "Additive manufacturing of 3D nano-architected metals," *Nature Commun.*, vol. 9, no. 1, p. 593, Dec. 2018.

MICHAIL E. KIZIROGLOU (Senior Member, IEEE) received the Diploma degree in electrical and computer engineering from the Aristotle University of Thessaloniki, Greece, in 2000, the master's degree in microelectronics and nanoelectronics from the Democritus University of Thrace, Greece, in 2003, and the Ph.D. degree in microelectronics and spintronics from the University of Southampton, in 2007. He is a Research Fellow of the Optical and Semiconductor Devices Group, Imperial College London. His research interests include energy harvesting devices, microengineering, and energy-autonomous wireless sensors.

BURAK TEMELKURAN received the M.S. and Ph.D. degrees from the Department of Physics, Bilkent University, Turkey, in 1996 and 2000, respectively. As a Postdoctoral Researcher at MIT, from 2000 to 2002, he has contributed to the discovery of the 1-D omnidirectional reflecting fiber. He is a Research Fellow of The Hamlyn Centre for Robotic Surgery, Imperial College London, U.K. He joined The Hamlyn Centre, in 2016, and his research is targeting unmet needs in medicine, with his expertise in the field of multimaterial fibers and with his 15 years of experience in the industry bridging engineering and medical sciences. His invention has been used in over 300 000 surgeries to date, mostly helping cancer patients. His research led to several foundational publications that pioneered the field of multimaterial fibers. He led the technology transfer process of this fiber to a start-up company. His research interests include the applications of multimaterial fibers and fiber robotics in medical robotics, sensors, and therapeutics.

ERIC M. YEATMAN (Fellow, IEEE) received the B.Sc. degree from Dalhousie University, Canada, in 1983, and the Ph.D. degree from Imperial College London, in 1989. He is currently a Professor of micro-engineering and the Head of the Department of Electrical and Electronic Engineering, Imperial College London. His research interests include motion and thermal energy harvesting for wireless devices, pervasive sensing, and sensor networks. He is a Fellow and Silver Medalist of the Royal Academy of Engineering and is a Cofounder and the Director of Microsaic Systems that develops and markets miniature mass spectrometers for portable chemical analysis.

GUANG-ZHONG YANG received the Ph.D. degree in computer science from Imperial College London, London, U.K. He is currently the Director of the Institute of Medical Robotics, Shanghai Jiao Tong University, Shanghai, China, and he was the Director of The Hamlyn Centre for Robotic Surgery, Imperial College London, from 1999 to 2019. He is a Distinguished Lecturer of the IEEE Engineering in Medicine and Biology Society, a Fellow of the Royal Academy of Engineering, IET, AIMBE, IAMBE, MICCAI, BSN, and City of Guilds, and a recipient of the Royal Society Research Merit Award and The Times Eureka Top 100 from British Science. He was the Editor-in-Chief of the IEEE Journal of Biomedical and Health Informatics and currently is an Editor of *Science Robotics*.